ABSTRACT

MORRISS, MATTHEW CONNOR. Dynamic and Tectonic Landscapes in Eastern Oregon Reveal Neogene to Quaternary Rearrangement of Topography. (Under the direction of Karl W. Wegmann).

Eastern Oregon contains the deepest canyon in North America, where the Snake River cuts the 2300 m deep Hells Canyon. A landscape that can maintain such a topographic features with high relief is likely undergoing relatively recent deformation. Study of the Burnt River, a tributary to the Snake, yielded data on river incision in eastern Oregon, indicating that Quaternary faults are a first order control on landscape development. Through 1:24,000-scale geologic mapping, a 500,000 year record of fluvial incision along the Burnt River was constructed and is chronologically anchored by optically stimulated luminescence dating and tephrochronology analyses. A conceptual model of fluvial terrace formation was developed using these ages and likely applies for other non-glaciated catchments in eastern Oregon. Mapped terraces, inferred to have formed during glacial-interglacial cycles, provide constraints on rates of incision of the Burnt River. Incision through these terraces indicates that the Burnt River is downcutting at a rate of 0.15– 0.3 m kyr^{-1}. This incision appears to reflect a combination of local base level adjustments tied to movement along the newly mapped Durkee fault and regional base level control imposed by the downcutting of the Snake River. Deformation of terraces as young as 38.7 ± 5.1 ka indicates Quaternary activity along the Durkee fault and when combined with topographic metrics (slope, relief, hypsometry, and stream-steepness) indicates a landscape in disequilibrium. In addition to deformation associated with the newly mapped Durkee fault, lithospheric dynamics (delamination and crustal foundering) initiated in the Miocene Epoch may be responsible for continued regional deformation of the Earth's surface.

Dynamic and Tectonic Landscapes in Eastern Oregon Reveal Neogene to Quaternary Rearrangement of Topography

by
Matthew Connor Morriss

A thesis submitted to the Graduate Faculty of
North Carolina State University
in partial fulfillment of the
requirements for the degree of
Master of Science

Marine, Earth, and Atmospheric Science

Raleigh, North Carolina

2015

APPROVED BY:

_____
Dr. Karl W. Wegmann
Committee Chair

_____ _____
Dr. Elana L. Leithold Del R. Bohnenstiehl

DEDICATION

To my supportive friends and family.

To Sarah Wolfe and Katie Lowe, two wonderful women I am so grateful are in my life.

To Rich Wiley and Rex White, two Raleigh friends without whom I never would have finished.

To Karl – for trusting me.

BIOGRAPHY

Matthew was born in Dallas, Texas but spent his formative years in Austin. Influential high school science teachers pushed him towards the sciences and in particular geology. A love of climbing drove him west. He received a B.A. in Geology and Climbing from Whitman College in Walla Walla, Washington in May of 2013. He then moved to the Piedmont of North Carolina to study a region of relatively unknown geology in eastern Oregon. Continuing to find his mind and body drawn to mountains, Matthew jumped on many a plane west, and after two months of summer research, he spent a month-and-a-half climbing and hiking in Alaska and British Columbia. Matthew is engrossed in his research in eastern Oregon and will continue some of the thought processes he has outlined in his Masters as a PhD student at the University of Oregon; however, he leaves North Carolina enriched by his time and experience in a new place full of amazing people.

ACKNOWLEDGMENTS

I would like to acknowledge my friend and advisor Dr. Karl Wegmann. What originally started as conversations over field-work in Mongolia has transformed into an all-consuming intellectual venture. I couldn't have asked for a better advisor. I worked hard because I loved the material but also because Karl fosters trust and hard work in his graduate students. Despite feeling disconnected from some of the work going on in our research group, I always felt welcome to discuss exciting ideas with Karl. My biggest regret in leaving North Carolina State University is leaving Karl.

This research began three years ago, and I intend to continue it at the University of Oregon. But it has grown through input from those around me. Dr. Robert Carson at Whitman College provided numerous ideas at the initial stages of this project. Jason McClaughry and Mark Ferns from the Oregon Department of Geology and Mineral Industries aided throughout my summer field work. Claire Vezie from Whitman College provided invaluable insights and patience throughout Field Work, and Skye Cooley provided counsel on several days of field work. His field insights were greatly appreciated. I also cannot thank Francis Mikan enough for first getting me excited about Geology. His high school lessons continue to inform my scientific process.

I would also like to thank the graduate students of North Carolina State University whom I am grateful to for ideas and company: John Wall, Steve Smith, Gantulga Bayasgalan, Nathan Lyons, Doug Czajka, Mike Mohr, Lisa Babuin, Nate Farrington, Angel Cruz, Adam Walters, and Stephen Hughes. Additionally, while we never overlapped at

NCSU, Sean Gallen has provided both enthusiasm and ideas relevant to this work. Thank you Sean for always being supportive and informative!

My parents are also to blame for my success in Graduate School. I greatly appreciate their support and willingness to entertain my much needed sanity-giving breaks in the mountains. I also wouldn't have been able to survive North Carolina without two great housemates; thank you Skyler Bunn and Eli Typhina for two good years of a warm home to come back to.

This research was supported by a U.S. Geologic Survey EdMap grant. Claire Vezie of Whitman College also provided field support, patience, and constant enthusiasm. Additionally, without exposures provided by 19th and 20th century gold miners, this study would have been nearly untenable. We are all thankful for their unending search for wealth.

TABLE OF CONTENTS

LIST OF TABLES

LIST OF FIGURES

LIST OF APPENDICES

CHAPTER 1: INTRODUCTION

The first and second deepest river gorges in North America (Hells Canyon of the Snake River and the Salmon River canyon) come within 20 km of each other in eastern Oregon and western Idaho. The single largest obstacle to rail traffic from Chicago, Illinois to Portland, Oregon is the relatively low-profile Blue Mountains on the Oregon-Idaho border. How is it that these topographic barriers are contained in an area with a radius less than 100 kilometers? This study examined in detail a tributary of the Snake River in an attempt to answer this question and detail the geomorphology and tectonics active within this tributary, inferring what other processes may be at work.

The ~2850 km^2 Burnt River Basin contains normal faults, Neogene volcanics, and Quaternary fluvial terraces, all of which indicate a dynamic late Cenozoic landscape. The Burnt River (BR) drains into the Snake at the upstream end of Hells Canyon. The Snake River (SR) represents the regional base level; any fluvial signal of the carving of Hells Canyon may have been communicated to tributary systems such as the Burnt River. The goal of this investigation from the outset was to improve our understanding of Neogene surface deformation in eastern Oregon (Fig. 1).

No previous investigation has examined eastern Oregon for signs of dynamic topography, where the elevations of modern landscapes are in part controlled by lithosphere-asthenosphere interactions. Herein, dynamic topography is defined as non-hydrostatic topography, or the topography that remains when isostatic responses or density variations are subtracted. Hales et al. (2004) and Darold and Humphreys (2013) suggest a mechanism for

such long wavelength mantle-supported surface deformation in the region through foundering of over-thickened lithosphere that was underplated to the base of North America in the Eocene. The hypothesized influx of hot asthenosphere and change in buoyancy of the post-delamination lithosphere might have created long-wavelength surface deformation or "dynamic" topography (e.g. Braun, 2010). The forcing of the continental surface upward by mantle processes may explain a diverse range of regional phenomena in eastern Oregon, including drainage reorganization of rivers, cutting of aforementioned canyons, and the spatial distribution of uplift and subsidence (e.g. Pierce and Morgan, 1992; D'Agostino et al., 2001; Hales et al., 2005; Wegmann et al., 2007; Gallen et al., 2013)

Detailed mapping of Quaternary deposits along the Burnt River (Fig. 2) constrain the rate and timing of fluvial incision, revealing a 500 ka record of incision in the lower and upper Burnt River canyons (Fig. 3A). Our mapping indicates that the Durkee fault, an active normal fault defining the Durkee Basin (Fig. 3A), controls the base level for the upper BR catchment. Given the deformation of terraces in the upper and lower BR canyons, local faulting is believed to drive much of the fluvial incision through this high relief landscape.

Neogene incision in the lower Burnt River canyon is interpreted as a combination of base-level adjustments tied to the Snake River and footwall uplift as the Burnt River exits the Durkee Basin (Fig. 3A). The trend and size of these faults is inconsistent with Neogene extensional tectonics (i.e. Basin & Range) in the western U.S (McCaffrey et al., 2013). It is possible that the Durkee fault formed due to a combination of rotational extension and long wavelength lithospheric flexure (McCaffrey et al., 2013).

CHAPTER 2: REGIONAL GEOLOGIC SETTING (PALEOZOIC AND MESOZOIC)

The study region encompasses accreted Paleozoic and Mesozoic terranes (Figs. 1, 4). Below is a brief outline of existing knowledge of the accreted terranes relevant to deconvolving the tectonic, dynamic, and volcanic components preserved in the topography and landforms of the Burnt River catchment. The Burnt River cuts through the Permo-Jurassic Baker Terrane, the Jurassic Izee Terrane, and clips the edge of the Triassic Olds Ferry Terrane (Dorsey and Lamaskin, 2008). These accreted terranes taper into the Salmon-River suture, marking the edge of the North American Craton (Fig. 4) and are the result of several accretionary events throughout the Mesozoic, forming the backdrop against which all Cenozoic activity is juxtaposed (Lamaskin et al., 2009).

The upper Burnt River canyon (Fig. 3A) is cut through the Triassic Burnt River Schist of the Baker Terrane (Ashley, 1995). The river then crosses the Durkee fault where it enters the Durkee Basin, which is filled with Miocene to Pliocene lake sediments (Van Tassell et al., 2001). The river once again crosses the Durkee fault as it enters the lower Burnt River canyon (Fig. 3). It then encounters the terrane bounding - and in some regions reactivated Connor Creek fault, transitioning from the Baker Terrane into the Jurassic Izee Terrane (Fig 3A; Dorsey and Lamaskin, 2008). Bedrock in this reach of the river is dominated by the steeply dipping Weatherby Formation (Dorsey and Lamaskin, 2008). The Burnt River crosses into the Permo-Triassic volcanic and volcaniclastic rocks of the Olds-Ferry Terrane and Huntington Arc, just before it enters the Snake River (Brownlee Reservoir; Silberling, 1987).

It is important to note that the accreted crust is juvenile in composition and rheological behavior when compared to the crust of the North American craton to the east of the $^{87}Sr/^{86}Sr$ 0.706 isopleth (Pierce and Morgan, 2009). Terrane accretion is the beginning of cratonization. The evolution of these terranes (delamination and topographic upheavals) is outlined in subsequent sections. Their relatively thin (crust ~25 – 35 km; lithosphere 55 – 60 km) nature when compared to the thicker craton (crust > 35 km; lithosphere ~80 km) to the east plays an important role in controlling both the spatial location of volcanism and the development of regional topography (Fig. 5; Camp and Hanan, 2008; Pierce and Morgan, 2009; Rodriguez and Sen, 2013; Hopper et al., 2014).

2.1 Cenozoic Evolution

The geologic history of Oregon extends beyond the Cenozoic; however, the bulk of the rocks exposed in the state are volcanic in origin and erupted within the past 40 Ma. The specifics of what volcanism occurred when, and why, is not the focus of this review; however, a select series of events is intimately connected with the development of topography in eastern Oregon. There are also a number of paleotopographic indicators that are volcanic in nature and have implications for understanding regional Cenozoic rearrangement of topography. The major events relevant to eastern Oregon are outlined in Figure 6 with geographic references in Figure 7. The eruption of the Yellowstone Plume at the McDermitt Caldera (ca. 16.6 Ma) initiated a phase of intense and extensive volcanism across Oregon, Washington, and Idaho (Cummings et al., 2000). In addition to the

subsequent eruption of the Columbia River Basalts, many other volcanic and tectonic events both pre and postdate these flood basalts (McClaughry et al., 2014).

2.2 Paleogene

After the docking of exotic terranes in the Mesozoic between c. 165 to 120 Ma, the next largest tectonic event to take place on the western margin of north America was the accretion of the Siletz terrane at approximately 50 Ma (Duncan, 1982; Dorsey and LaMaskin, 2007; Dorsey and Lamaskin, 2008; Lamaskin et al., 2009, 2014). Farallon slab subduction accelerated between accretion events, resulting in Sevier thin-skinned thrusting coeval with intrusion of the Idaho batholith (Gaschnig et al., 2010). The subduction of warmer and more buoyant oceanic lithosphere forced a shallowing in subduction angle that initiated an amagmatic period in the Idaho and Sierra Nevada batholiths and concomitant large thick-skinned thrust-faulting in the Wyoming province (Miller et al., 1992; DeCelles, 2004).

Both the Sevier and Laramide orogenies resulted in high standing orogenic topography to the east and south of Oregon. Between 48 and 39 Ma, areas 50 to 100 km due east of Hells Canyon may have stood at an elevation of 3700 m above sea level, as recorded in the $\delta^{18}O$ of hydrous authigenic minerals in paleosols, whereas present elevations in this region are between 2000 and 2500 m (Mix et al. 2011). Rocks of the Precambrian Belt Super Group formed the drainage divides between major east and west-flowing Eocene Rivers (Allen, 1991; Sears, 2014). These through-going fluvial systems appear to have survived subsequent Paleogene and early Neogene volcanism. These paleochannels continue to exert

a control over the landscape of eastern Oregon and northern Idaho to this day, despite tectonic rearrangement of drainages in the Neogene. Fluvial channel-bed conglomerates consisting of Proterozoic quartzite and Eocene Challis volcanic clasts occur at elevations of ~3000 m in eastern Oregon mountain ranges (Fig. 7; Allen, 1991).

Foundering and removal of the Farallon flat slab from beneath western North America initiated Cascade arc volcanism (45 to 40 Ma) and is coincident with the initiation of extensive silicic extrusive volcanism across what is now the Basin and Range physiographic province, including the eruption of the Clarno (45 to 40 Ma) and John Day volcanics in eastern Oregon (~40 Ma to 21.5 Ma; Fig 6; Humphreys, 1995; McClaughry et al., 2009).

2.3 Neogene

The topography and outcrops of eastern Oregon record the culmination of volcanic and dynamic topography, fault controlled extensional basin formation, the filling and draining of large lakes, and the carving of some of the world's deepest canyons all in the interval between the cessation of John Day volcanism at ~21.5 Ma to eruptions at Cinder Butte (0.8 to 1.9 Ma; Fig. 7). Because of the diverse suite of Neogene geologic deposits and landforms, regional paleotopography in the region can be directly measured in places and estimated in others. This study provides an overview of the development of topography throughout the Neogene in northeastern Oregon.

2.4 Columbia River Basalts

Volcanism in southeast Oregon initiated at 16.8 Ma with the eruption of the McDermitt Volcanic field and Steens Basalts (Fig. 8). Both were associated with the interaction of the Yellowstone mantle plume with the base of continental lithosphere (Fig. 9; Hooper et al., 2007; Ferns and McClaughry, 2013). After these initial eruptions, the locus of basaltic volcanism propagated to the north. Despite the Yellowstone Plume impacting North American lithosphere in south-eastern Oregon, the Columbia River Basalts erupted far to the North of this location, paralleling the edge of cratonic North America (Hooper et al., 2002; Rodriguez and Sen, 2013; Ferns and McClaughry, 2013).

Two different mechanisms have been invoked as the cause of this northward migration, since a link between the Steens Basalts, Columbia River Basalts, and the Yellowstone Plume was first proposed by Hooper (1982). The average rate of eruptive center migration from south to north is faster than both plate motion and mantle convection (10 to 100 cm yr^{-1}), requiring another physical mechanism to match this observations (Camp and Ross, 2004). Darold and Humphreys (2013) suggest from their modeling of recently acquired tomographic data that a piece of oceanic lithosphere underplated eastern Oregon and Washington in the Paleogene (Fig. 9A). This oceanic lithosphere appears to have delaminated into the underlying asthenosphere and is used in two competing hypotheses that explain the origin of the Columbia River Basalts.

Darold and Humphreys (2013) propose that the Yellowstone plume initiated delamination along the contact between the continental and remnant underplated Farallon

lithospheres. The resulting northward-directed foundering of this "slab" enabled the introduction of plume asthenosphere to the bottom of the continental lithosphere. With tractive forces akin to those occurring during the process of slab rollback, the plume head was drawn northward as the lithosphere continued to founder, with a final hinge located beneath southeastern Washington (Darold and Humphreys, 2013).

Ascending plume asthenosphere contacted the hydrated continental lithosphere, resulting in the melt that would erupt as the Columbia River Basalts. At approximately the same time, the ultramafic root of the Wallowa Batholith is hypothesized to have detached from the crust in the form of a Rayleigh-Taylor instability between 16 and 15 Ma – just after delamination of the Farallon slab (Hales et al., 2005; Darold and Humphreys, 2013). This second, more isolated density-driven delamination event may explain the topographic swell associated with the Wallowa Mountain uplift and surrounding basins that help to define a circular array of topography (e.g. Hales et al., 2005).

Camp and Hanan (2008) present a different model of plume development and northward migration without a foundering slab of oceanic lithosphere (Fig. 9B). In this model, basal lithospheric topography across the ancestral North American craton boundary was exploited by a buoyant plume head that migrated "uphill" to the north. Both of these models invoke significant plume/lithosphere interactions to explain the northward time-transgressive eruption history of the Columbia River Basalt Group. Regardless of which of the two main competing hypotheses is correct, such strong lithosphere/asthenosphere interactions are expected to create significant geomorphic (Earth-surface) response (e.g. Becker et al., 2013).

2.5 Other Volcanic Units

Eruption of the Dooley Volcanics in the study area occurred at roughly the same time (~14.7 Ma) as the Frenchman Springs flows of the CRBG (Figs. 6 and 7; Ferns and McClaughry, 2013). These rhyolite ash-flow tuffs are nearly 1000 m thick and have only been dated in two locations. The Powder River Volcanics (Figs. 6 and 7) are a small group of basaltic-to-rhyolitic eruptive centers and flows that overlie and interfinger with the CRBs (Bailey, 1990). These flows and vent deposits span an area of nearly 100 km (north-south) in eastern Oregon and have a geochemical signature that is consistent with the Darold and Humphreys (2013) lithospheric-foundering hypothesis (Nicolaysen et al., 2014). For several other volcanic units beyond the purview of this review, see Ferns and McClaughry (2013).

2.6 Neogene Basins

Extensional basins began opening in eastern Oregon and western Idaho as volcanic units were erupting. Normal faulting initiated on the north-south trending Oregon-Idaho graben (OIG) at 15.3 Ma and continued until 12.6 Ma (Cummings et al., 2000). The end of active extension along the OIG coincided with the initiation of faulting responsible for the formation of the internally-drained Boise Basin at 11 Ma (Wood and Clemens, 2002). The sedimentary deposits associated with this large lake (Lake Idaho) are herein called Lake Idaho deposits (Wood and Clemens, 2002). This lake, the size of Lake Huron, was long-

lived (10 to 1.7 Ma) and may have been connected to other basins in northeastern Oregon (Van Tassell et al., 2001). The modern Snake River upstream of Hells Canyon drains the area once inundated by Lake Idaho.

Several other basins in northeastern Oregon began to open by 4 Ma (Baker Basin, Grande Ronde Valley, Pine Valley, and perhaps the Durkee Basin; Van Tassell et al., 2001). The history of Lake Idaho is tied to these depositional basins and to Hells Canyon, which has long been viewed as the outlet for the lake (Wheeler and Cook, 1954). Two competing hypotheses have been put forward for the spillover of Lake Idaho into Hells Canyon. The Wood and Clemens (2002) hypothesis (Hyp. 1 in Figure 6) suggests that Lake Idaho overtopped a sill and began discharging into Hells Canyon or was captured by headward erosion of the Mio-Pliocene Clearwater-Salmon River at ~4 Ma (Reidel and Tolan, 2013b). The lake continued to exist and lacustrine units were deposited until 1.7 Ma (Wood and Clemens, 2002). In a competing hypothesis (Hyp. 2 – Fig. 6), Van Tassel et al. (2001), suggest that fluvial units and fossils recovered in drill cores from the Grande Ronde Valley (GRV) indicate that there was a possible outlet stream connecting Lake Idaho to the GRV in route to the lower reach of Hells Canyon.

The Van Tassel et al. (2001) hypothesis is based upon the similarity between fossil fish fauna (*Lavinia, Acrocheilus*, and *Klamathella*) in the GRV and Boise Basin. Van Tassel et al. (2001) asserts that a connection between Lake Idaho and Hells Canyon was established no later than ~2 Ma based on the disappearance of the deep-water diatom *Stephano discus* assemblages from the Baker Basin and GRV. This younger age for the outlet of Lake Idaho is reasonable as Lake Idaho sedimentation ended in the Boise Basin at 1.7 Ma; however, the

lacustrine history of Lake Idaho is complicated by lake level and land elevation change. The lake level lowered by at least 300 m at ~6 Ma, only to fill again to a new high stand of 1200 m (Wood and Clemens, 2002). The lake level lowering event at 6 Ma recorded inferred by Wood and Clemens (2002) may signify the capture of Lake Idaho through Hells Canyon as outlined in Hypothesis 1; however, if the lake was captured successfully by the Snake River at 6 Ma, why then would the lake rise again to an even higher level until 1.7 Ma? On the other hand, does a younger 1.7 Ma capture event leave enough time for incision of Hells Canyon? The geologic history of the late Neogene Period in this region is a complex story of not only volcanic units, but also, tectonism, lacustrine deposition, and fluvial records.

2.7 Quaternary

During the Quaternary Period, eruptions of several basaltic cones and flows occurred at Cinder Butte, which is located along the southern divide of the Burnt River catchment (Figs. 6 and 7). These 1.9 to 0.8 Ma flows conformably overlie lake sediments, providing a local datum and upper time horizon for a lake that just pre-dated their eruption (Ferns and McClaughry, 2013). Quaternary valley glaciers in the Wallowa and Elkhorn Mountains formed cirques, widened and deepened valleys, and constructed large moraine complexes at the front of both ranges (Crandell, 1967; Ferns et al., 2010). The geologic forces active in the region throughout the Neogene, including dynamic topography, tectonics, and volcanism have all left different marks on the landscape. This study is focused on the fluvial geomorphic indicators of these active processes in the Burnt River catchment (Fig. 2).

CHAPTER 3: METHODS

A combination of Digital Elevation Model (DEM) analysis of the 10 m resolution National Elevation Dataset and detailed fieldwork were used to investigate the development of topography in Eastern Oregon. The ~2850 km^2 Burnt River drainage basin is ideal for a geomorphic study because unlike other rivers in the greater Hells Canyon region, the entire catchment is accessible by roads. Preliminary topographic analysis of the drainage basin indicated a long wavelength convexity in the river longitudinal profile (Fig. 10) that suggested that a portion of the basin was in disequilibrium due to either tectonic or longer wavelength dynamic influences. We sought to deconvolve these two possibilities.

Field analysis focused on the upper and lower Burnt River Canyons (Fig. 3A). A key component of this project was locating and determining the specific elevation of the bedrock surfaces (straths) below terrace gravels. Comparing strath elevations to the modern river profile and to other terraces allowed for the measurement of the amount and rate of fluvial incision within both canyons (e.g. Bull, 2009). Surficial travertine deposits, landslides, alluvial fans, pediments, alluvial units, and anthropogenically-modified sediments (Fig. 11) were also mapped to better understand the late Quaternary evolution of the Burnt River catchment.

3.1 Terraces

Fluvial terraces are landforms and deposits that integrate tectonic, climatic, and geomorphic processes at the watershed scale (Bull, 1990; Pazzaglia, 2013). Different forms

of terraces (strath or fill) develop through a predominance of tectonic or climatic forcings. The strath is a planed bedrock surface, which at a point in the past was the bottom of a river channel. It represents the basal unconformity upon which alluvium is deposited. A strath terrace consists of a thin veneer (1 to 3 m) of sediment capping a strath surface. This alluvial cap is the thickness of sediment in motion during large discharge events (Wolman and Miller, 1960). A fill terrace is a thick deposit representing extensive aggradation or burial of the river valley and raising of the channel bed. Both strath and fill terraces are topped by the bench-like "tread." The alluvium found between the strath and tread are the terrace deposits. Several mechanisms for the creation of strath and fill terraces are discussed below. The type of terrace that was most important and relevant to the study of incision along the Burnt River in northeastern Oregon is elaborated upon in both the Results and Discussion sections.

Internal (autocyclic) mechanisms have been suggested as possible drivers for the formation of strath terraces (e.g. meander migration, meander cutoff, and landslides (e.g. Finnegan and Dietrich, 2011). With constant incision, streams will establish channel gradients that allow for movement of all bedload supplied to the system (Bull, 1990, 1991). When the rate of horizontal river incision (meandering) is greater than the vertical incision, the lateral beveling of a bedrock strath surface occurs (Wegmann and Pazzaglia, 2002; Montgomery, 2004). The lateral to vertical rate of incision is thought to be driven by both internal and external controls (Hancock and Anderson, 2002; Wegmann and Pazzaglia, 2009). Bedload sediments are the tools of the stream that are needed to bevel a strath. These beveling processes continue until tectonic or climatic forces change stream power (discharge) or sediment supply (Bull, 1990). With renewed down-cutting, a river abandons the strath and

alluvial deposits in the landscape above the modern (now lower in elevation) channel that is inset into the hillslope as a marker of where the river channel used to be.

Fill terraces begin to form when hillslope sediment influx is greater than stream competence, resulting in aggradation. Channel aggradation buries the previously cut strath, creating a new, higher tread surface. Fill terraces likely represent times of climatic change when more material is delivered from hillslopes to the channel. Tectonic activity expressed as regional uplift, propagation of base level fall accommodated through migrating knickpoints, or an increase in stream power due to climatic change can tip a stream from aggradation to degradation and cutting (Bull, 1991; Zaprowski et al., 2001; Cook et al., 2013). With an increase in power, streams will incise through the thick accumulation of alluvial fill, stranding fill terraces in the landscape (Bull, 1990).

It is commonly assumed in tectonic geomorphology studies that the gradient (river longitudinal profile) of a paleo-strath surface (strath terrace) was similar to the modern channel profile for bedrock, or mixed bedrock alluvial rivers (e.g. Pazzaglia and Brandon, 2001). Before any correlations between straths and the modern channel are made, however, the modern channel is examined under the assumption that it currently represents the long-term equilibrium profile of the river in question (Wegmann and Pazzaglia, 2002). A vertical incision rate can then be calculated from the height of a strath terrace above the modern river as long as the age of the terrace deposits are known or can be estimated. For the two canyons of the Burnt River, terrace strath surfaces and deposits are well exposed by the hydraulic mining activities of the late 19th and early 20th century gold miners. However, aggradation of the modern channel bed of the Burnt River in response to the influx of terrace and

hillslope sediment liberated by these mining activities means that incision rate calculations along the Burnt River are minima, as bedrock is not exposed anywhere along the channel today, and thus the height differential between a terrace strath and the modern strath is unconstrained. Geotechnical and water wells were exploited in the lower Burnt River canyon to approximate the position of the modern strath.

Recent models of terrace development (e.g. Pederson et al., 2006; 2013; Gallen et al., 2015) imply that incision rates calculated between straths, rather than between a strath and the modern channel, represent a more precise estimate of long-term fluvial incision rates. Rates determined between a strath and the modern channel may overestimate Quaternary incision rates because the position of a river channel in space does not represent a fixed datum with respect to the geoid – a requirement for the proper measurement of rate-dependent processes such as river incision (Gallen et al., 2015). Rate calculations between observed terraces and the modern channel cannot capture the full elevation history of the streambed; therefore derived rates contain inherent biases. For the purposes of this study, incision rate calculations will be made between terraces and when possible, between terraces and the modern channel strath as constrained by data from water and geotechnical borings.

3.2 Field Methods

This study focused on the landforms and geomorphology of the upper and lower Burnt River canyons (Fig. 3A). These two locations coincided with the steeper segments of the Burnt River longitudinal profile and with steeper tributary streams (Fig. 10, 12).

Geologic mapping took place in May and June of 2014. Mapping efforts were aided by late 19th and early 20th century gold miners, who exposed terrace alluvium in both the upper and lower Burnt River canyons (Fig. 11). Terraces were located and strath surface elevations were measured. Radiocarbon, tephrochronology, and optically-stimulated luminescence (OSL) samples were opportunistically collected. Observations of weathering rind thickness from basalt cobbles (Fig. 13A) and the relative degree of granite-cobble grussification provided relative age control for different terrace levels. The degree of development of soil Bt and Bk horizons within the terrace deposits at different elevations above the modern channel were noted in addition to the overall thickness of the deposits.

Hydraulic mining activities in and along the Burnt River exposed not only terrace deposits but also often the strath surface itself (Figs. 13B and 13C). Key outcrops exposed along the lower Burnt River canyon were visible in road cuts (Fig. 13D). Strath surface elevations were measured using a Trimble GeoXH 2008-series differential GPS system. Absolute elevations of measured strath surfaces were often resolvable to ± 0.15 m (Appendix A). At locations where the strath was not exposed, a minimum or maximum elevation was measured to provide reference to terraces up and down stream. Except in a few places with limited line of sight, a TruePulse laser range finder was used to measure the height of each strath above the modern Burnt River to within ± 1 m.

3.3 Tephrochronology

Terrace deposits exposed by recent mining activity in the upper Burnt River canyon contained an intact tephra (Fig. 14). A sample of this tephra was collected and analyzed at the Peter Hooper GeoAnalytical Lab at Washington State University (WSU) by an automated Siemens X-Ray powder diffractometer for major oxide constituents, (SiO_2, Al_2O_3, Fe_2O_3, TiO_2, K_2O, MgO, CaO, and Cl). The elemental profile from the Burnt River sample was compared for chemical similarity to the WSU tephra database (n = 1716). For a detailed description of the WSU tephrochronology and geochemistry procedures, see Johnson et al. (1999). Additional research yielded an age of 201 ± 45 ka for this tephra (Kuehn and Negrini, 2010).

3.4 Optically Stimulated Luminescence

Samples of fine-grained sand were collected from fluvial terrace deposits for OSL dating (Fig. 15). Sampling procedures followed a standard outlined by the University of Utah OSL Laboratory (http://www.usu.edu/geo/luminlab/how2osl.pdf). Samples were processed at the University of Georgia Luminescence Dating Laboratory. Carbonate and organics were removed with a 10% HCl and 20% H_2O_2 treatment. Samples were sieved to isolate the 125-150 μm, 150-180 μm, and 180-250 μm grainsize fractions. Heavy liquid (2.65 g cm^{-3}) was used to separate feldspars. The resultant separate was etched with 40% HF and cleaned with 10% HCl.

OSL measurements were made using an automated Risø TL/OSL-DA-15 reader, with a mounted $^{90}Sr/^{90}Y$ source and a dose rate of 0.085133 Gy/s (Markey et al., 1997). The quartz dose rate was measured following the Single Aliquot Regenerative protocol outlined in Murray and Wintle (2000). The in-situ dose rate (a product of radioactive decay in the environment proximal to the sample) was calculated using additional samples of sediment from each site. Dose rate calculations were made using a Daybreak alpha counting system to estimate U and Th concentrations. For a detailed description of lab methods, see http://osl.uga.edu/technique.html and Srivastava et al. (2005). Sample water content was assumed to be ~8 ± 4%, which is within a normal range for elevation, climate, and sample type. The cosmic ray dose rate was estimated using sample elevation, depth, and latitude (Prescott and Hutton, 1994).

3.5 Remote Sensing

DEM analysis of regional topography was conducted prior to field work to select priority sites. The longitudinal profile of the Burnt River was extracted from the 10 m resolution National Elevation Dataset. TopoToolbox 2, a MATLAB native script package, was used almost exclusively for all topographic analyses (Schwanghart and Scherler, 2014). Topographic data were used to calculate normalized stream steepness (k_{sn}). This normalized value refers to the steepness of a certain fluvial reach, normalized for the upstream drainage area (Kirby and Whipple, 2001; Kirby et al., 2003). K_{sn} is calculated using the following equation:

$$K_{sn} = k_s A^{(\theta ref - \theta)} \qquad (eq.\ 1)$$

where k_s is the channel steepness index, A is the median upstream area from an examined stream segment, and Θ_{ref} is a reference channel concavity, usually the mean for channels in the region without knickpoints or tectonic disturbances, or in most cases Θ_{ref} is calculated over the entire catchment of interest (Wobus et al., 2006). Θ_{ref} generally ranges from 0.35 to 0.65 (Kirby and Whipple, 2001; Wobus et al., 2006). Θ is the channel concavity as calculated from regression through a log-log plot of local slope versus contribution drainage area. For this examination of the Burnt River, a k_s of 22.73 was applied and a Θ of 0.409 was measured from the regression through the curve of the logarithmic slope-area plot.

The upper Burnt River canyon coincides with a steeps segment of the river's longitudinal profile (Fig. 10) and a zone of high tributary and main channel K_{sn} values (Fig. 10) coincide with the upper Burnt River canyon. Normalized channel steepness indices (K_{sn}) were calculated via TopoToolbox for all sub-catchments within the Burnt River basin that drain areas ≥ 12 km^2 and with channel lengths ≥ 2 km. The K_{sn} data were then exported as a shapefile and smoothed in ArcGIS (Fig. 10) with a moving mean using a 100 m window, similar in approach to the analyses of Miller et al. (2013).

ArcGIS was used to calculate relief within the Burnt River catchment (Fig. 3C) with a circular 100 m moving window. A slope raster was calculated using built-in DEM processing routines (Fig 3B). The possibility of a transient disequilibrium signal or knickpoint, traveling up the Burnt River catchment was examined further using logarithmic slope-area plots and hypsometric curves (generated with the use of TopoToolbox 2) from

seven select tributaries (Fig. 16). The hypsometric integral (HI) was calculated for each sub-catchment by:

$$HI = (Z_o - Z_{min})/(Z_{max} - Z_{min}) \qquad (eq.\ 2)$$

where Z_o, Z_{max}, Z_{min} are the mean, maximum, and minimum elevations within the basin of interest. The hypsometric integral is an easy-to-calculate value that stands in as a proxy for tectonic activity, indicating when catchments are steeper and undergoing active incision or have eroded to equilibrium (Keller and Pinter, 2002). Higher HI values (≥ 0.5) are often interpreted as indicating disequilibrium within a catchment either from tectonic activity or a migrating transient imparted from one or more knickpoints responding to base level fall (Pike and Wilson, 1971; Keller and Pinter, 2002).

3.6 Lake Idaho sediments as a paleotopographic datum

The presence of presumed Lake Idaho deposits within the Burnt River catchment serve as a potential paleoaltimetric control. Wood and Clemens (2002) estimated a maximum surface elevation of 1,100 m for Lake Idaho in the Boise Basin, based on the highest modern elevation of lake sediments. Wood and Clemens (2002) speculate that this high stand occurred at approximately 4 Ma. If tectonic or dynamic rearrangement of topography within the past 4 Ma is presumed to be negligible within portions of the Burnt River catchment, then the highest elevation of Lake Idaho sediments provide a datum from which a gross incision rate for the lower Burnt River canyon may be calculated. We interpret

these incision rates as minimums as there has likely been erosion of lake deposits and some tectonic activity in the intervening time.

On Dixie Creek (Fig. 3), a horizontal basalt flow caps Lake Idaho deposits. This basalt flow and its eruptive edifice are likely part of the latest series of basaltic volcanism in the region known as the Kivett Sequence (Ferns and McClaughry, 2013). The youngest flows in the Kivett sequence are between 0.1 to 2.2 Ma (Ferns and McClaughry, 2013). These Quaternary flows provide a chronologic constraint on the incision of Dixie Creek and an absolute topographic constraint, but only a minimum age constraint. If the lakebeds are in fact older than 2.2 Ma, the resulting incision rate would be slower.

CHAPTER 4: RESULTS

4.1 Terrace Stratigraphy

Geomorphic mapping along the Burnt River revealed seven distinct fluvial terrace levels with intact strath surfaces in the upper canyon and five in the lower canyon (Figs. 17A and B; Appendix - B). Additional terrace deposits were located, photographed, and mapped; however, deposits without an exposed strath were not included in the long-profile terrace correlations presented on Figure 17. Terraces are denoted from oldest-to-youngest as $Qt1_U$ to $Qt7_U$ in the upper Burnt River canyon and from $Qt1_L$ to $Qt5_L$ in the lower canyon (Fig. 17). Modern exposures of terrace deposits most often coincide with sites of late 19th and early 20th century hydraulic gold mining. For this examination, the upper and lower Burnt River canyon terraces will be treated separately, as the Durkee Basin is the local base level for the upper Burnt River canyon. In some cases, 1 to 2 m of alluvial cover above the strath unconformity remained intact (e.g. had not been entirely stripped off by hydraulic mining activities; Figs. 11 A and E). Terrace alluvium commonly fined upward from cobble to boulder-sized clasts at the strath – terrace contact, to overbank deposits of sandy silt (Fig. 14A). Terrace deposits are most commonly covered by varying thicknesses of younger, locally-derived colluvium (Fig. 13D).

The only indications of the oldest and highest terraces (> 100 m above the modern river) in both the upper and lower Burnt River canyons are isolated, well rounded cobbles found at hillside mining excavations. The presence of greenstone, quartzite, and deeply weathered basalt clasts that are different from underlying bedrock (Fig. 13A) are the only

sign of former fluvial processes associated with the highest terraces ($Qt1_U$, $Qt2_U$, $Qt1_L$, and $Qt2_L$). These old terraces contained no dateable material and their overlying, presumably cumulic, soils were removed by mining activities. Geochronologic constraints from the younger terraces ($Qt5_U$, $Qt3_L$, and $Qt5_L$) are provided by a geochemically matched tephra (Fig. 14), optically stimulated luminescence ages (Fig. 15), and correlation of soil profiles development to a regional chronosequence developed for the Palouse Hills in the Columbia Basin (Fig. 18).

Strath surfaces are constructed out of a mix of competent rock units throughout the length of the Burnt River. In the upper canyon, straths are composed of both Burnt River Schist and the Nelson Marble (Ashley, 1995). In places bedrock flutes and potholes associated with erosion of the former riverbed are still visible on the strath surfaces that have been exposed in two dimensions by hydraulic mining (Fig. 13C). Downstream of the Conner Creek fault, straths are often cut into and across the near vertical foliation of the Weatherby Formation (a metamorphosed flysch unit; Lamaskin et al., 2009). Terrace map patterns indicate that they are unpaired along the length of the Burnt River. The topographic expression of the majority of the identified terraces in the upper and lower canyons is subdued, at best. The terraces were difficult to identify, as their narrow treads (and deposits) were covered with local colluvium that resulted in little change in hillslope gradient above buried terrace and strath pairs. Terrace identification would be more difficult without the historic hillslope hydraulic mining activities.

4.2 Upper Burnt River Canyon

In the upper Burnt River canyon, four of the seven mapped terraces appear to correlate across a significant distance ($Qt3_U$ to $Qt7_U$). The upper Burnt River canyon provided only one reliable geochronometric constraint: the tephra collected in the fine-grained overbank facies deposits of $Qt5_U$ (Fig. 14). The Peter Hooper GeoAnalytical Lab at Washington State University identified the Burnt River $Qt5_U$ terrace tephra as a geochemical match to the 160 ka Paoha Island tephra, originating from Mono Craters in eastern California (Table 1; Williams, 1994**)**. A sample of fine sand to silt-sized quartz-bearing fluvial sediment was gathered for OSL analysis from the Qt4 terrace just upstream from the terrace with the preserved tephra. This terrace is stratigraphically higher and therefore older than the Qt5 terrace. The University of Georgia OSL lab returned an age of 81.59 ± 9.61 ka (Table 2); however, this OSL determination is inconsistent with the tephrochronology of the lower $Qt5_U$ terrace. Subsequent research revealed that the 160 ka age estimate for the Paoha Island tephra has been updated to ~201 ± 47 ka (Kuehn and Negrini, 2010). With a high level of confidence in the tephra identification (≥95%) and previous dating of the Paoha Island tephra to 201 ± 47 ka, the $Qt4_U$ OSL sample is excluded from further analyses. The calculated incision rate at river km 56 for the $Qt5_U$ terrace (29.6 ± 1.0 m above the modern river) using the Paoha Island tephra age of 201 ± 47 ka is 0.15 ± 0.03 m ka^{-1} (Table 4).

Reconstructed terrace longitudinal profiles from the upper Burnt River canyon are approximately parallel to the modern channel profile (Fig. 17A). The one exception is a large step in the $Qt3_U$ terrace sequence. This step correlates with an incised cutoff meander

bend in the upper canyon. The river gradient before the meander was cutoff is preserved in the three uppermost $Qt3_U$ terraces. The pre-cutoff river was at least 1.8 km longer and had a gradient of (~0.001) over a distance of 6 km, as preserved by $Qt3_U$ terraces (Fig. 17A). The gradient of the modern river across the same reach is ~0.004. One additional explanation for the disparity between the gradient of the modern river and that of $Qt3_U$ is that during times of meander growth, fluvial incision ceased (e.g. Finnegan and Dietrich, 2011). The section of the $Qt3_U$ terraces with a lower gradient appears to correlate with a more sinuous reach section of the Burnt River (Fig. 17A). Lateral channel migration may have outpaced incision, resulting in a lower gradient channel. There is also a possible difference in the erodibility between the Nelson Marble and Burnt River Schist. If the Marble is more erodible than the schist, it is possible that the river will cut to a lower gradient profile faster through the marble than through the schist. The contact between the two units is unmapped, but it may be between river kilometer 62 and 59 (Fig. 18A; Appendix - B; Brooks, 1979b; Ashley, 1995). However, this explanation alone does not explain the observed lower channel gradient as the younger $Qt4_U$ and $Qt5_U$ terraces do not exhibit similarly low gradients.

4.3 Lower Burnt River Canyon

Only three terraces ($Qt3_L$ to $Qt5_L$) exhibit mappable continuity along the length of the lower Burnt River canyon. Two optically stimulated luminescence samples provide a chronology of incision for the lower Burnt River canyon during the past 90 ka. The fine-grained deposits in a $Qt3_L$ terrace returned an age of 84.74 ± 13.93 ka (Fig. 17; Table 2),

while a sandy lens from a $Qt5_L$ terrace yielded an OSL age of 38.68 ± 5.13 ka (Table 2). Sediments from other terrace deposits were collected for radiocarbon dating; however, a lack of recoverable organic material rendered them useless for this purpose. The two OSL constraints provided a long-term incision rate for the lower Burnt River canyon (Table 4). To account for possible channel aggradation caused by late 19th to early 20th century gold mining activities, we first calculated the incision rate between the $Qt3_L$ and $Qt5_L$ terraces (Table 4). The calculated rate of incision from this comparison is 0.31 ± 0.05 m ky^{-1} (Table 4). The rate of incision measured directly from the $Qt5_L$ terrace to the modern channel is 0.21 ± 0.16 m ky^{-1}. However, water and geotechnical wells drilled in the lower Burnt River canyon provide enough data to estimate that 3 to 5 m of historic aggradation has occurred above the modern bedrock strath surface of the Burnt River (Table 3). This alluvial thickness can then be added into the overall height of terraces above the modern pre-mining channel. The incision rate between the $Qt5_L$ terrace and the bedrock below the alluvium is 0.31 ± 0.07 m kyr^{-1}. This rate is comparable to the incision rate calculated between the $Qt3_L$ and $Qt5_L$ terraces.

The longitudinal profiles of the three correlated terraces in the lower canyon are approximately parallel to the modern Burnt River channel for the lower 25 km above the Snake River confluence. However, with increasing proximity to the Durkee Basin, the gradients of the $Qt4_L$ and $Qt3_L$ terrace profiles increase in comparison to the modern river channel. The modern channel gradient (0.004) is roughly equivalent to the gradient of $Qt5_L$ (0.004), $Qt4_L$ (0.003), and $Qt3_L$ (0.005) downstream of the over-steepened reach (Fig. 17, 18; Table 5). The $Qt4_L$ gradient is 0.008 (Table 5). This deflection may be due to footwall uplift

on the Durkee fault (see Discussion section). While there are not enough data points to precisely determine the gradient of the $Qt3_L$ terrace sequence, these older terraces appear to be deformed to a still steeper gradient. Increasing terrace gradient with age is expected with the accumulation of throw along the Durkee fault.

A model of terrace formation was constructed in order to provide estimates for the ages of undated terraces, and thus fluvial incision rates along the length of the Burnt River. See the Discussion section for more details on this conceptual model of terrace development.

4.4 Paleo-elevation Metrics

The current elevations of Miocene-to-Pliocene lacustrine sediments in the Burnt River catchment provide a minimum elevation for paleo-Lake Idaho in and around the Boise Basin, as well as a possible mechanism for measuring post-Lake Idaho surface deformation. The modern landscape position of these sediments within the lower Burnt River canyon was used to measure long-term incision at two locations. Above Huntington, Oregon (2 km upstream of the confluence of the Burnt and the Snake Rivers), lakebeds are mapped to ~850 m (Fig. 20; Appendix - D). This elevation is a minimum for the true lake surface as sedimentation would not initiate at the extreme edges of the lake and there may have been erosion and/or burial of lacustrine sediments at higher elevations since the draining of Lake Idaho. The confluence of the Burnt and Snake Rivers is at 634 m (prior to the flooding of the Brownlee Reservoir). The 1,100 m hydraulic highstand of Lake Idaho occurred at approximately 4 Ma (Wood and Clemens, 2002). The modern elevation of Lake Idaho sediments and their reported ages provide enough constraints to measure a minimum average

incision rate of 0.54 ± 0.01 m ky^{-1}) since the late Pliocene to early Quaternary from near to the mouth of the modern Burnt River (Table 4).

Pliocene basalt flows of the Kivett Sequence (Hooper et al., 2002) overlie Lake Idaho sediments in the mid-reaches of Dixie Creek (Fig. 3), providing another chronostratigraphic constraint on fluvial incision in the Burnt River basin. The base of the oldest basalt flow exposed on the north flank of Table Rock overlies Lake Idaho sediments at 1250 m (Fig. 3). The proximal modern elevation of Dixie Creek is 780 m. Available geochronology for the Kivett basalt flow is limited to three $^{40}Ar/^{39}Ar$ ages: 0.8 ± 0.7 Ma, 1.7 ± 0.1 Ma, and 1.9 ± 0.3 Ma (Hooper et al., 2002). For the purposes of this analysis, these three ages were treated as a single possible range for the age of the Table Rock flow (~ 1.15 ± 1.05 Ma). The lava flows adjacent to Dixie Creek have not been dated; therefore, it is possible that they could be older than ~2.2 Ma. Based on flow morphology, it is unlikely to be younger than 100 ka. The estimated time-integrated rate of incision for Dixie Creek since emplacement of the Table Rock basalt flow on top of Lake Idaho sediments is 0.4 ± 0.3 m ky^{-1} (Table 4).

4.5 Hypsometric Indices

To further quantify landscape development within the Burnt River catchment, sub-basins were examined in detail for evidence of tectonic activity. The seven largest catchments feeding the Burnt River exhibit three different hypsometric and slope characters (Fig. 16). Sub-catchments 1, 2, and 3 have slightly steepened to nearly flat hypsometric

curves. Mean slopes are between 15 and 20° over the majority of each sub-basin, with elevation evenly distributed throughout. Catchment 2 contains a large area of lakebeds capped by pediment surfaces. These pediments are likely responsible for the high percentage of area with low elevations (1200 to 1400 m) and low slope (5 to 12°). The hypsometric integrals for these three sub-basins range from 0.31 to 0.44.

The second grouping of catchments (4, 5, and 6) display much steeper hypsometric curves and are all proximal to, or directly flow into the Durkee Basin. These three catchments maintain the highest hypsometric integral values observed across the entire BR basin (0.55 to 0.59). Catchments 5 and 6 have two distinct elevation-area peaks, which correspond to zones of both high and low elevations that exhibit low slopes (10 to 15°). Catchments 3 and 4 join the Burnt River at the steepest section along its longitudinal profile (Fig. 10).

The hypsometric curve for catchment 7 is most similar to basins 1, 2, and 3; however, this basin has a higher hypsometric integral (0.48) and maintains a larger area at higher slopes (≥ 20°) than sub-basin 1, 2, and 3. Catchment 7 is also the largest sub-basin in the lower half of the Burnt River basin. This catchment is diverse in bedrock lithology. It also contains two Quaternary volcanos (Cinder Butte and Table Rock; Fig. 3).

4.6 Soil Geochronology

Hydraulic mining removed most terrace deposits and their overlying soils throughout the upper and lower Burnt River canyons. Without intact terrace stratigraphy, estimating a

relative chronology based upon pedological properties was not feasible. One exception is a 7-m thick $Qt3_L$ terrace deposit in the lower Burnt River canyon that contains both a modern and buried soil, each with its own pedogenic carbonate horizon (Fig. 18). The lower, older soil contains a Btkb horizon with stage 3-plus carbonate accumulation, while the upper (modern soil) exhibits only stage 2 Bk horizon development (Gile et al., 1965). Both the modern and buried soils developed within thick loess deposits. The soils demarcate intervals of reduced atmospheric silt loading to the site and relative landscape stability. Two mature soils and the presence of weathering rinds (≥ 5 cm) on basalt cobbles and complete grussification of granite clasts in the terrace deposits below the soils indicate the advanced age of this deposit (Fig 13B).

Soil stratigraphy in the Palouse Hills of eastern Washington is well constrained for the past 100 ka (see McDonald et al. 2012, and references therein). The Btk soil in the $Qt3_L$ deposit likely correlates to the Washtucna Soil in the Palouse Hills (MIS 2, ~24 ka). The underlying soil that contains the stage 3-plus Btkb horizon may correlate to the Devils Canyon Soil (MIS 4, ~60 to 70 ka; McDonald et al., 2012). This proposed soil chronostratigraphy supports the 84.7 ± 13.94 ka OSL age collected in the flood overbank sands directly beneath the lower, buried soil (Fig 18).

4.7 Evidence for Active Faulting in the Durkee Basin

The Durkee Basin separates the upper and lower canyons. The basin is filled with Miocene to Pliocene lake deposits. A formerly active pediment surface truncates these basin

fill deposits (Fig. 22). The pediment surface is now incised into by transverse streams. Ashley (1995) mapped a normal fault on the southwest margin of the Durkee Basin (see Figure 12.2 of that publication). Ashley only extended the fault along part of the mountain front, and to date, no other geologist has chosen to extend the fault along the entire mountain front on the margin of the basin. Yet, several pieces of evidence point toward the presence of a Quaternary fault that bounds the south side of the Durkee Basin. The evidence for this fault includes the following observations: (1) Triangular facets are found along a NW-SE striking trend, demarcating a linear mountain front (Fig. 21). (2) Eight springs are mapped along the mountain front – piedmont interface on USGS 7.5-minute topographic quadrangle maps. (3) Outcrops of travertine found in three locations along the mountain front, indicate the presence of long-lived springs (Fig. 22). A ridge of travertine exposed in the basin was presumably deposited in a paleo-valley; therefore, topographic inversion has taken place within the basin (Figs. 11D & 22). (4) Tributary streams to the Burnt River are significantly steeper along the southern limit of the Durkee Basin, as they cross the fault (Fig. 12) and normalized channel steepness (k_{sn}) values from these tributaries decrease with distance from the Durkee Basin and its bounding fault. The steep and shallow stream gradients are within the same lithology (Nelson Marble) so lithological variation alone cannot explain observed changes in stream steepness. However, a normal fault active within the Durkee Basin would drop base level for these tributaries and account for steep stream reaches proximal to the fault with gentler gradients further from the fault. These areas with gentler stream gradients may represent pre-faulting topography. (5) The $Qt4_L$ and $Qt3_L$ terrace profiles seen in the lower Burnt River canyon steepen with increasing proximity to the Durkee Basin (Table 4; Fig. 17,

19). These terraces are on the footwall of the Durkee fault. Given that footwall uplift typically accounts for 20 percent of total throw on extensional faults, each displacement of the Durkee fault (earthquake) would uplift terraces relative to the Burnt River, and this uplift would be maximized closest to the fault (Stein et al., 1988).

A topographic swath along the mountain front in the Durkee Basin indicates a decrease in topography towards the ends of the 16 km long fault, with 0.5 km of footwall displacement (Fig. 23). The highest topography along a recently active normal fault is often observed toward the fault mid-section as maximum displacement typically occurs farthest from the fault tips (e.g. Dawers et al., 1993). The swath profile in the Durkee Basin shows such a signature (Fig. 23) with the greatest mountain front relief located in a mid-fault position that then tapers towards the fault tips.

Fault-scaling relationships can be used to calculate the maximum possible moment magnitude (M_w) of an earthquake given slip along the entire surface trace of the Durkee fault following the Wells and Coppersmith (1994) regression equation:

$$M_w = 5.08 + 1.16\log(SRL) \qquad (3)$$

where SRL is the surface rupture length, estimated at a maximum of 16 km for the Durkee fault. Using this equation, the Durkee fault is estimated to produce at maximum a ~6.5 Mw earthquake during a complete 16 km-long rupture event.

4.8 Evidence for Active Faulting at the Mouth of Clarks Creek

The confluence between Clarks Creek and the Burnt River marks both the upstream end of the upper Burnt River canyon and the location of an unmapped, northwest-trending down-to-the-south normal fault (Fig. 3A). This fault is likely neither as large nor as recently active as the Durkee fault. We present evidence for the existence of this Clark Creek fault based on the following observations. (1) There is a distinct topographic transition at the mouth of Clarks Creek (Fig 3A). The broad alluvial Bridgeport valley abruptly ends and the upper Burnt River canyon begins where the stream crosses the fault. A normal fault would explain such a rapid change in topography. (2) Clarks Creek flows northwest; the Burnt River flows northeast. At the mouth of Clarks Creek, water in the channel takes a 90° turn to the east to join the Burnt River. Clarks Creek is the only major tributary to join the Burnt River that flows in the opposite direction to the main stem, which is consistent with fault-control of the local drainage pattern. (3) The ~14 Ma Dinner Creek tuff dips to the southwest and steepens into Clarks Creek (Ferns, personal communication, 2014). This increase in dip is consistent with the existence of the Clarks Creek fault, presently concealed beneath the alluvial valley floor.

CHAPTER 5: DISCUSSION

High standing topography in eastern Oregon and western Idaho is dissected by two of the deepest gorges in North American (the Hells and Salmon River canyons). Such features initially seem incongruous with existing hypotheses for their development, namely that either preferential drainage capture and erosion along the strike of small range-bounding normal faults (e.g. Vallier, 1998), or spill-over across a low topographic sill from Lake Idaho resulted in the carving of Hells Canyon (Wood & Clemens, 2002). Neither of these models integrate published concepts of regional lithospheric processes and development during the past 16 Ma (e.g., Hales et al., 2005; Camp & Hanan, 2008; Darold & Humphreys, 2013). During the mid-to-late Cenozoic, eastern Oregon and western Idaho were impacted by the passage of the Yellowstone plume, likely leading to lithospheric delamination of underplated oceanic lithosphere (Darold and Humphreys, 2013), and the probable foundering of an ultra-dense crustal root from beneath the Wallowa batholith (Hales et al., 2005). This investigation sought to deconvolve local tectonic deformation from possible longer wavelength signal(s) of the aforementioned lithosphere-asthenosphere dynamics as observable in the landscapes and fluvial networks of northeastern Oregon. This study has produced a model for terrace formation in unglaciated basins of northeastern Oregon, providing possible ages for previously undated terraces in the region.

5.1 The Burnt River

A field investigation of fluvial terraces along the Burnt River reveals a two-fold story of river cutting and active faulting within the catchment. It appears that incision by the Burnt River is driven by two processes: (1) movement along a previously unmapped fault in the Durkee Basin and (2) base-level adjustments tied to the Snake River. Prior to initiating the field-mapping component of this study, we hypothesized that down cutting along the Snake River resulted in propagation of a base-level fall signal into the Burnt River catchment, as manifested through the broad convexity in the Burnt River longitudinal profile that is coincident with the two 500-m-deep gorges in the basin (Fig. 3A; 10). The Burnt River is a tributary to the Snake River upstream of Hells Canyon. A kinematic wave of incision from the cutting of Hells Canyon was hypothesized to have propagated through the Burnt River catchment. Upon mapping the catchment, the aforementioned evidence indicates that movement on the previously unmapped Durkee fault is likely responsible for the observed convexity and incision of the Burnt River through the upper canyon. The lower canyon likely formed as a combination of incision through the uplifting footwall of the Durkee fault in addition to keeping pace with the dropping Snake River. The Burnt River is a prime location to investigate regional landscape incision as it is accessible by vehicle, in contrast to the Hells Canyon reach of the Snake River. In addition, widespread 19th and 20th century hydraulic gold mining exposed terrace deposits along the length of the Burnt River.

5.2 Terrace Genesis Model

The following model of terrace formation was constructed to provide approximate ages for undated terraces along the Burnt River. The model integrates newly dated terraces from this study with previously published estimates of terrace ages from the Owyhee River of southeastern Oregon, and the Middle Fork of the Salmon River in central Idaho. The three dated terraces in the Burnt River catchment – $Qt5_L$, $Qt3_L$, and $Qt5_U$ – are aligned with interstadials (Fig. 24). $Qt5_L$ corresponds to the latter part of MIS 3; $Qt3_L$ to late MIS 5 to early MIS 4, and $Qt5_U$ to late MIS 7. The conceptual model described below follows a framework wherein strath formation occurs during interglacial intervals (MIS 3, late 5, and late 7) with the Burnt River aggrading during glacial times (MIS 2, 4, and 6).

The incision responsible for capturing these strath terraces in the landscape above the main channel requires a change in the fluvial character of the Burnt River. Either a decrease in sediment load with constant stream power or an increase in stream power with constant sediment supply drives a river to cut through its own strath. Late Quaternary climatic cycles provide the necessary environmental controls on the Burnt River catchment, either by sapping the river of alluvium during times of strath formation and degradation, or flooding the channel with colluvium, leading to aggradation. Uplift across the Burnt River catchment throughout these climatic shifts allowed for continued river incision, stranding terraces as high as 90 m above the active channel (Fig. 17). Close examination of interstadial (MIS 3, 5, and 7) climate in the Pacific Northwest (PNW) provides an internally consistent model for the behavior of the Burnt River that led to the formation of the observed terraces.

MIS 3 was a period of cool and moderate precipitation, comparable to the modern climate of the PNW (Fig. 24; Whitlock and Bartlein, 1997; Grigg and Whitlock, 2002; Herring and Gavin, 2015). Late MIS 5 was a time of warmer and moister climate than is found today in the PNW (Whitlock and Bartlein, 1997; Herring and Gavin, 2015). MIS 7 was a period of warming similar to MIS 5e when sea surface temperatures rose off the PNW coast and terrestrial precipitation increased (Lyle et al., 2001). Pollen records indicate that the PNW was dominated by a *Picea* (spruce) and *Pinus* (pine) forest during MIS 3 and 5a (Whitlock and Bartlein, 1997; Herring and Gavin, 2015). MIS 2 and 4, times of colder and drier climate in the PNW, were dominated by the *Artemisia* genus of shrubs and *Poaceae* family of grasses (Whitlock and Bartlein, 1997; Herring and Gavin, 2015).

MIS 3, 5a, and 7 were times of forest expansion throughout the PNW. There may have been dense, deep-rooted vegetation along the hill slopes above the Burnt River during these intervals. The dominance of tree cover in the Burnt River catchment during MIS 3, 5a, and 7 in combination with a moist climate favors the creation and retention of colluvium on hillslopes (Bull, 1991). The Burnt River was starved of hillslope sediment and likely in contact with bedrock during these periods, moving only a thin (1 to 3 m) veneer of alluvium. A moist climate ensured ample stream power with which to carve an extensive strath surface, which would subsequently be incised, preserved in the landscape, and mapped as part of this study.

Glacial times in the Burnt River catchment (MIS 2, 4, and 6) were likely dry and dominated by shallow rooted grasses and shrubs. The climatically-driven transitions in flora likely resulted in decreased hillslope stability and increased movement of hillslope material

into the river channel. A drier climate would also hinder soil formation. Processes such as rain drop erosion and sheetwash due to decreased infiltration rates became important forces of erosion, driving material down hillslopes (Bull, 1991). More sediment in the main channel increased the resistance to fluvial processes, and the Burnt River began to aggrade. Other catchments in the Pacific Northwest experienced large fluxes of sediment due to glacial activity during stadials (see Pazzaglia and Brandon, 2001). No part of the Burnt River basin was ever glaciated, meaning that the river was entirely at the behest of precipitation and tectonics to supply sediment downstream. Lack of glaciers in the headwaters of the Burnt River may explain why there are no large accumulations of valley fill from stadial aggradation periods. It seems likely that the Burnt River was raised off its strath due to the influx of sediment beyond the transport capacity of the river; however, in comparison to formerly glaciated basins aggradation along the Burnt River channel was much less significant.

Based on existing geochronology and aforementioned paleoclimate constraints, straths appear to have formed during interglacial intervals and were likely incised through during the transition into glacial times, before valley aggradation began. Previously undated terraces can now be associated with cycles in marine $\delta^{18}O$. $Qt4_L$, $Qt2_L$, $Qt3_U$, $Qt1_L$, $Qt2_U$, and $Qt1_U$ have all been tied with glacial-interglacial cycles (Fig. 24), providing a best-fit model for both available geochronology and paleoclimate data.

This model also correlates with other terraces observed in catchments to the south and east of the Burnt River (Fig. 2, 7; 24). Ely et al., (2012) described several terraces along the Owyhee River in southeastern Oregon. While a longer record of terrace development

was not available from the Owyhee, the Dogleg T4 and T5 terraces overlap in age with $Qt5_L$ in the Burnt River catchment. These terraces were dated using ^{3}He cosmogenic radioncludes to 45 ± 3 ka (T5) and 39 ± 3 ka (T4), or roughly mid-MIS 3 (Ely et al., 2012). These ages correlate, within error, to the $Qt5_L$ terrace sequence dated to 38.68 ± 5.13 ka in the lower Burnt River canyon (Fig. 17). The Middle Fork of the Salmon River, the only other nearby catchment with previously studied strath and fill terraces, appears to share a similar terrace chronostratigraphy to the Burnt River (Fig. 24; Meyer and Leidecker, 1999). However, the large errors inherent in the basalt weathering rind technique employed by Meyer and Leidecker (1999) makes any direct correlation problematic. The two data points from the Owyhee study corroborate new geochronology on terraces along the Burnt River. There is not enough good data from Meyer and Leidecker (1999) to make firm conclusions about regional terrace formation. Further study could yield more evidence of an interglacial degradation and glacial aggradation sequence in eastern Oregon.

5.3 Durkee Fault Mechanics

The above model of terrace development allows a previously undated terrace ($Qt4_L$) to be used to determine the amount of slip along the Durkee fault. Neither the $Qt5_L$ nor the $Qt3_L$ terraces provide enough data points to properly measure deflection resulting from footwall uplift. However, five outcrops define the Qt4L terrace in the 10 km downstream from its projected intersection with the Durkee fault. The reconstructed longitudinal profile of the fault-proximal portion of the $Qt4_L$ terrace increases in gradient in comparison to the

$Qt4_L$ terrace further downstream in the lower Burnt River canyon (Fig. 17, 19). Extending the deformed and undeformed $Qt4_L$ profiles until they intersect with the fault plane provides an estimate of the total vertical footwall displacement of the Durkee fault since terrace formation (Fig. 19). The reconstructed position of the $Qt4_L$ strath is 46 ± 4.6 m higher than it would be without fault deformation. The error on this measurement is provided by allowing for a 10% variance in terrace gradient. The estimated age for $Qt4_L$ from our regional terrace genesis model is ~55 ± 5 ka, resulting in a total footwall displacement estimate of 0.8 ± 0.1 mm yr^{-1} for the Durkee fault (Table 6).

Fault movement may not be the only explanation for increased terrace gradients near to the Durkee Basin. The modern profile of the Burnt River is also over-steepened along the same reach (~ river km 27 to 37; Fig. 19). The uppermost 10 km of the lower Burnt River canyon is over-steepened by 7° from the rest of the Burnt River profile in the canyon. The modern Burnt River is ~ 19 ± 1.9 m higher when it reaches the fault plane than if the downstream gradient of 0.004 was maintained throughout the canyon (Fig. 19). Earthquake-related footwall uplift would steepen the river through this section; however, this steeper section of the profile could also be controlled by lithologic variations in rock hardness that manifest themselves through variations in channel gradient (Fig. 21). As the river exits the Durkee basin, it flows across the Nelson Marble for ~ 10 km before encountering the Weatherby Formation. The 10 km reach underlain by the Nelson Marble is steeper and less sinuous than the remainder of the lower Burnt River canyon. The different rock types along the lower Burnt River canyon (marble versus shale) may offer a first-order control on channel steepness. There is currently no way of parsing out whether or not some component

of the observed over-steepening is tectonic; however, it seems likely that the Burnt River is at or actively cutting to a mostly pre-earthquake profile as there are no signs of recent ruptures in the Durkee basin (i.e. a fault scarp). Employing this operating assumption, the modern downriver profile gradient is used to normalize this 10 km reach for possible bedrock control.

Subtracting the aforementioned over-steepening of the modern channel from the $Qt4_L$ terrace yields 27 ± 5 m of potential tectonic over-steepening of the channel profile adjacent to the Durkee fault (Table 6). Integrating the modeled terrace age (55 ± 5 ka) yields a revised footwall uplift rate of 0.5 ± 0.2 mm y^{-1}. Footwall uplift accounts for ~20% of total fault slip (e.g. Stein et al., 1998). Therefore, the maximum estimate of fault displacement from the $Qt4_L$ terrace within the past 55 ± 5 ka is 2.5 ± 1.0 mm y^{-1} (Table 6).

A topographic swath profile incorporating the Durkee fault-controlled mountain front allows for a maximum of 0.5 km of footwall displacement (Fig. 22). The Durkee fault has a maximum total displacement of 2.5 km, provided that the 80:20 ratio of hanging wall to footwall displacement holds true and there has been no reduction in footwall topography by erosion. It seems unlikely that the rate of slip would be constant through time; however, this study did not gather enough data to determine the total fault slip history. The minimum age of the Durkee fault is 1 ± 0.4 Ma, using a footwall displacement rate of 0.5 ± 0.2 mm $yr^{-1}$and a maximum footwall displacement of 0.5 km, and assuming no erosion of footwall topography (Table 6). Given the presence of Miocene to Pliocene lakebeds within the basin, it is likely that slip rates have varied through time and the basin is older than this estimate.

5.4 Burnt River Dynamics

Downstream of the observed over-steepened terraces, the lower Burnt River channel and the reconstructed terrace longitudinal profiles maintain a similar gradient (0.004) to the modern stream (Fig. 17, 19). Channel steepness (gradient) normalized to basin area (K_{sn}) is greater for the lower Burnt River canyon and adjacent tributary streams than the observed general trend of streams in the upper half of the Burnt River catchment (Fig. 12). K_{sn} values in the lower canyon tend to be >150, while channel reaches in the upper catchment are generally <150 (Fig. 12). These steeper streams are in the lower 32 km of the Burnt River catchment, between the Durkee Basin and the river's mouth. Additionally, slopes in the lower Burnt River canyon are steeper and relief is higher than in the majority of the upper Burnt River catchment (Fig. 3B & C). Footwall uplift along the Durkee fault alone cannot account for these observations. Through known fault-scaling relationships, footwall uplift should only account for ~5% of the total fault throw at a distance of 10 km from the fault plane for extensional faults (e.g. Stein et al., 1988). Over a distance of 30 km, the effect of slip along the Durkee fault would be negligible on channel and reconstructed terrace gradients. Additionally, streams are consistently steep throughout the lower Burnt River catchment; rather than only adjacent to the Durkee fault. Therefore, some process other than slip along this fault is responsible for incision of the main channel and its tributary streams as observed along the lower Burnt River canyon. Two explanations for these observations include: (1) a regional signal of uplift across the Burnt River catchment, or (2) a drop in base level tied to incision along the Snake River.

The first explanation, regional uplift, could account for several observations made within the Burnt River catchment. Despite slip along the Durkee fault creating the Durkee Basin, streams flowing across the fault have incised through basin sediments (see Appendix – C). Older Quaternary pediment surfaces preserved above the hanging wall of the Durkee fault indicate that streams were graded to a local base level of erosion, which was then lowered – perhaps through regional uplift or further down cutting of the Burnt River transmitted through the lower canyon. Streams responded, cutting through this pediment surface. One explanation for this observed incision on the hanging-wall side of a normal fault is uplift at a wavelength longer than the entire Durkee Basin. Wood and Clemens (2002) estimated the maximum elevation of Lake Idaho at 1100 m; however, within the Burnt River catchment late Miocene to Pliocene lacustrine sediments are mapped to an elevation of 1484 m (Robyn, 1977). Applying age constraints of the Lake Idaho high stand, the difference in maximum lake sediment elevations throughout the region represents a long-term uplift rate of 0.1 ± 0.02 m kyr^{-1} (Table 4).

This uplift could be responsible for the observed stream incision through hanging-wall sediments in the Durkee Basin and may play a part in continued incision in the lower Burnt River canyon. The mechanism responsible for this observed uplift could be the aforementioned geodynamic processes, still active below eastern Oregon (delamination and sinking of a plutonic root). This estimate is only that – an estimate. It likely represents a minimum rate as lacustrine sediments are easily eroded. The overall deformation due to uplift in the region might still be greater; however, the time-averaged uplift rates are unlikely to be higher than ~0.3 m kyr^{-1}. This upper bound on uplift in the region would place

lakebeds at ~2300 m, or the elevation of modern drainage divides between the John Day and Burnt River.

5.5 Hazards

The aforementioned geologic phenomena (faulting, volcanism, and landslides) pose a real geologic hazard to communities in eastern Oregon (see Appendix B, C, and D). The lower Burnt River canyon is a major conduit for both travel and energy resources. Interstate-84 and the only rail line in eastern Oregon both pass through this canyon. Additionally, a liquefied natural gas line goes through this corridor, and the Ash Grove Cement plant (the only cement plant in Oregon) is < 1 km from the projected plane of the Durkee fault. A surface rupture on this fault has the potential to damage all three transportation conduits as well as disrupt operations at the cement plant, which is the largest single employer in Baker County. Fault scaling relationships reveal that a rupture along the entire surface trace of the fault could produce an earthquake with a maximum moment magnitude of 6.5. Such an event would be damaging to existing infrastructure and surrounding communities. Additionally, the presence of large deep-seated landslides along the lower Burnt River canyon represents another threat to these energy and transportation corridors (Appendix – D). The geologic hazards within the Burnt River catchment should be integrated into assessments by regional transportation and energy officials.

CHAPTER 6: CONCLUSIONS

This study of the Neogene to Quaternary landscapes of eastern Oregon leads to the following conclusions based on mapped landforms, fluvial processes and existing geology. There are active normal faults within the Burnt River catchment that provide a local base level and drive fluvial incision of the upper Burnt River canyon, creating 700 m of relief in the process. The calculated incision rate for the fault controlled, upper Burnt River canyon based on 1:24,000 scale mapping and tephrochronology is 0.15 ± 0.03 m kyr^{-1}. The Durkee Basin formed as a result of down-to-the-northeast movement on an unmapped normal fault, herein called the Durkee fault. The Burnt River crosses this fault twice, creating two characteristically different fluvial reaches (the upper and lower Burnt River canyons). Major automobile and train traffic thoroughfares and a liquefied natural gas pipeline cross the Durkee fault. These transit and energy conduits are threatened by potential seismic activity along this normal fault. Footwall uplift along the Durkee fault is responsible for over-steepened terraces in the uppermost lower Burnt River canyon. Incision rates within the undeformed reach of the lower Burnt River canyon range from 0.31 ± 0.05 to 0.21 ± 0.16 m ky^{-1}.

New optically stimulated luminescence ages and tephra geochronology on mapped strath terrace deposits within the Burnt River catchment indicate that during interstadials, horizontal incision outpaced vertical incision. The observed strath terraces were likely captured in the landscape through incision at the transition between interstadials and stadials. The Burnt River was likely raised above its strath during stadial periods due to channel

aggradation. However, the Burnt River did not aggrade significantly as fill terraces do not exist in the catchment. Extensive fill terraces likely did not form in the Burnt River basin, as hillslopes, not glaciers, were the first order control on catchment sediment supply. This genetic model of terrace development in eastern Oregon is consistent with the sparse available river terrace data from other regional river systems. Additional studies of fluvial terraces in the region is warranted to build an even more robust model.

This study found that continued incision throughout the Burnt River catchment not associated with Durkee Basin faulting but may be due in part to long wavelength regional uplift at a rate of $\sim 0.1 \pm 0.02$ m kyr^{-1}. This rate was determined through assessing the displacement of late Miocene to Pliocene lake beds above the regional Lake Idaho high-stand elevation of 1,100 m. This uplift signal is 30 % of measured stream incision, and it represents only a minimum estimate of uplift since the lakebeds were deposited. Additional incision in the lower Burnt River canyon is likely tied to the regional base level that is set by the Snake River, which has cut a significant river gorge (Hells Canyon) downstream within the past 4 to 6 Ma. Further research in the region is warranted, as many questions regarding uplift and fluvial incision remained unsolved. This study represents only a preliminary dataset on the geomorphic landforms, paleotopographic datums, and rates of surface elevation change for east-central Oregon.

Table 1. Tephra identification results from the Peter Hooper Geoanalytical Lab at Washington State University. The tephra sample was based on the chemistry of 19 individual glass shards. The similarity coefficient refers to the chemical signature matching of the tephra sample with the Paoha Island Tephra**.**

Oxide Analyzed	Weight Percent
SiO_2	73.98
Al_2O_3	14.66
Fe_2O_3	2.30
TiO_2	0.19
Na_2O	4.47
K_2O	3.08
MgO	0.17
CaO	1.00
Cl	0.14
Total	99.99
Number of shards analyzed	19
Similarity Coefficient	0.95

Table 2. Optically stimulated luminescence (OSL) data from Burnt River terrace deposits.

Sample ID	Site	Elevations (m asl)	Dose Rate (Gy ky^{-1})[1]	Aliquot no.	De(Gy)[2]	Water Content (%)	OSL Age (kyr)[3]	OIS[4]
BRS14*	$Qt6_U$	963	-	-	-	-	-	-
BRS17	$Qt4_U$	1028	1.89±0.16	16	154.0 ± 12.8	8 ± 4	81.6 ± 9.6	5a
BRS8	$Qt5_L$	732	1.62±0.13	12	62.7 ± 6.5	8 ± 4	38.7 ± 5.1	3
BRS9*	$Qt4_L$	771	-	-	-	-	-	-
BRS12	$Qt3_L$	773	1.8±0.15	8	152.3 ± 21.8	8 ± 4	84.7 ± 13.9	5a

*BRS14 did not contain enough quarts to return an OSL age.

[1] Background dose rate (D_e) in Grays per 1000 yrs.

[2] Equivalent dose rate (D_e) in Grays.

[3] Optically stimulated luminescence age with error in 1000s of years before present.

[4] Oxygen Isotope Stage determined from deposit age.

Table 3. Available well data from the lower Burnt River canyon, indicating aggradation of the main channel possibly due to 19th and early 20th century mining activities. An average alluvium depth of 3.9 ± 0.4 m (assuming a 10% error) was used to correct incision rate calculations (Table 4).

Oregon Well ID	Latitude (°)	Longitude (°)	Elevation (m)	Depth to Bedrock (m)	Proximal river Elevation (m)	Estimated Alluvial fill (m)
Bake 52289	44.48494	-117.3423	720	12.2	712.6	4.8
Bake 52020	44.381505	-117.3033	661.8	6	658.8	3

Table 4. Incision and uplift rates calculated within the Burnt River catchment. The $Qt3_L$ terrace incision rate was calculated based upon the vertical separation between $Qt5_L$ and $Qt3_L$, not between $Qt3_L$ and the modern channel. The uppermost Lake Idaho deposits have been used in two places to measure overall incision and uplift, based on the Wood and Clemens (2002) hypothesis for an 1,100 m lake high stand at ~ 4 Ma.

Incision Indicator	Age (ka)	MIS[a]	Height of Strath above channel (m)	Incision rate (m/kyr)	Age Source
Qt5 (U)	201 ± 47	6	29.6 ± 2	0.15 ± 0.03	Paoha Island tephra[b]
Qt3 (L)[C]	84.7 ± 13.9	5a	-	0.31 ± 0.05	OSL
Qt5 (L)	38.7 ± 5.1	3	8 ± 2	0.21 ± 0.05	OSL
Qt5 (L)[D]	38.7 ± 5.1	3	11.9 ± 2	0.31 ± 0.06	OSL
Table Rock Basalt flow (Dixie Creek)	1500 ± 700	-	470 ± 12	0.4 ± 0.03	Ferns and McClaughry, (2013)
Lake Deposits at mouth of BR (L)	4000 ± 900	-	216 ± 12	0.05 ± 0.01	Wood and Clemens (2002)

Uplift Indicator	Age (ka)	MIS[a]	Change in Lake Bed Elevations (m)	Uplift rate (m/kyr)	Source
Mean change of Lake deposits	4000 ± 900	-	384 ± 15	0.1 ± 0.02	Robyn, (1977)

[a] OIS = Oxygen Isotope Stage.
[b] For tephrachronology see Kuehn and Negrini (2010)
[c] Incision rates for $Qt3_L$ were calculated in reference to the $Qt5_L$ terrace, not to the modern Burnt River channel.
[d] A second incision rate was calculated between $Qt5_L$ and the approximation of the bedrock channel elevation as determined from well logs.

Table 5. River and terrace gradients in the lower Burnt River canyon.

	Deformed Gradient	Underformed Gradient
Qt3	-	0.005
Qt4	0.008	0.003
Qt5	-	0.004
Modern River	0.006	0.004

Table 6. Displacement of the Durkee fault as calculated by deformation of $Qt4_L$ terraces. The minimum age for the Durkee fault has been calculated using the estimated maximum displacement of the footwall (Fig. 21) and the slip rate reported below.

	Offset (m)	Age (ka)	Rate of displacement (mm y^{-1})
Footwall Displacement	46 ± 4.6	55 ± 5	0.8 ± 0.1
Normalized* Footwall offset	27 ± 5.2	55 ± 5	0.5 ± 0.21
Hanging wall displacement (4 x footwall)	-	-	2.0 ± 0.84
Total Fault Displacement (5 x footwall)	-	-	2.5 ± 1.0

Durkee fault	Maximum footwall Displacement (mm)	Slip rate (mm/yr)	Minimum Fault age (Myr)
	500000	0.5 ± 0.2	1.0 ± 0.4

* Normalization was an attempt to subtract the effects of more resistant bedrock beneath the Burnt River. See Discussion section for details.

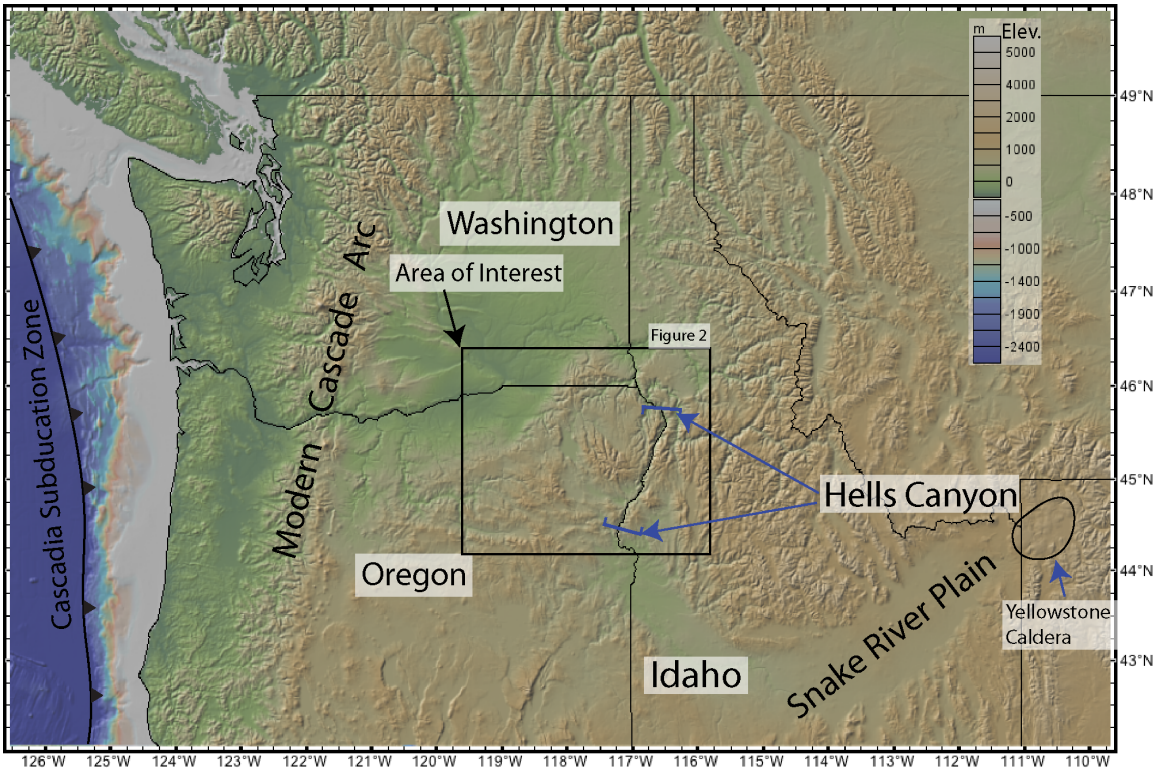

Figure 1. Highlighted study area near the triple point of Oregon, Idaho, and Washington. The area of interest is expanded in Figure 2. Elevation data is from the 30 m resolution National Elevation Dataset, displayed using GeoMapApp.

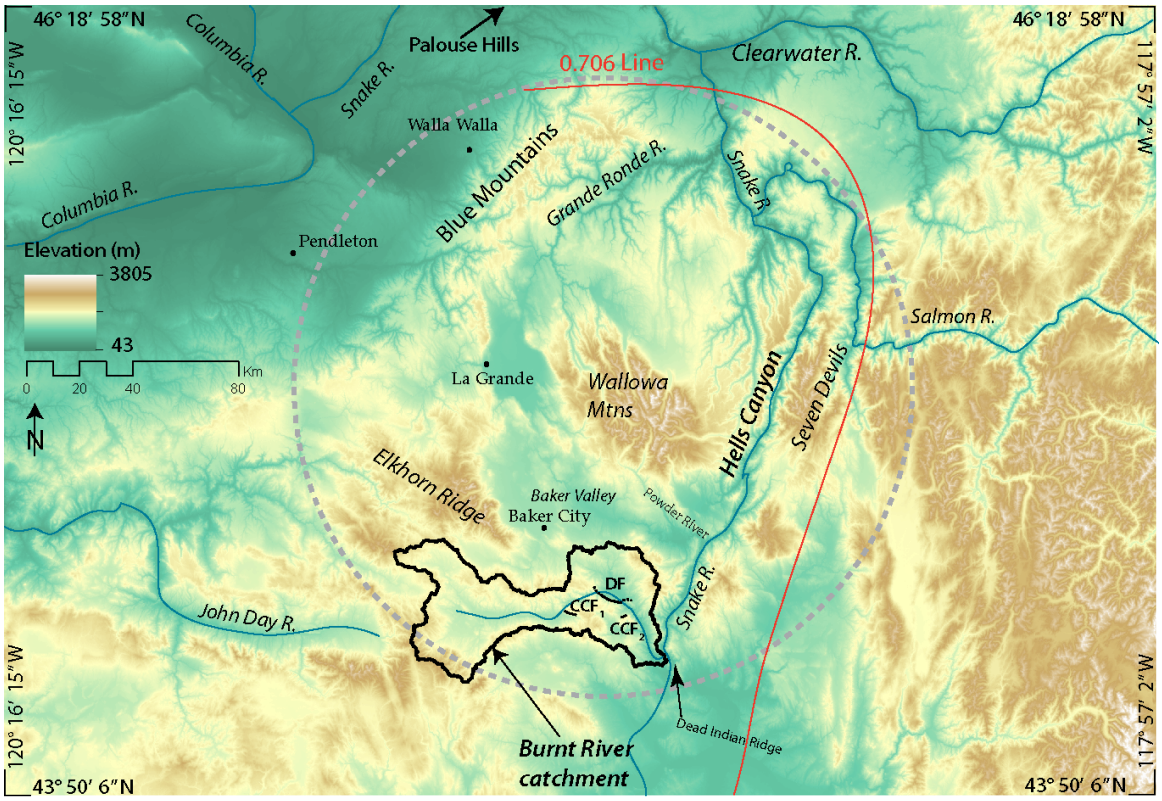

Figure 2. The Burnt River catchment (bold polygon) in the context of regional topography and drainage networks. The approximate boundary between the North American craton and accreted terranes demarcated by the $^{87}Sr/^{86}Sr$ 0.706 isopleth is shown by the thin red line (Leeman et al., 1992). The Bulls-eye of high topography described in Hales et al. (2005) and by Darold and Humphreys (2013) is outlined by the gray dashed line. Abbreviations include: DF for the Durkee fault; CCF_1 for the Clarks Creek Fault; CCF_2 for the Conner Creek Fault.

Figure 3. Topographic metrics of the Burnt River catchment **A**. Shaded relief map of the Burnt River catchment, using data from the 10 m National Elevation Database. The largest communities in the catchment (Unity, Durkee, and Huntington) are labeled. The Durkee Basin and its bounding fault (the Durkee fault) divide the upper and lower Burnt River canyons. **B**. Catchment slopes. A large portion of the steeper slopes are located in the lower half of the basin with the steepest slopes in the upper Burnt River canyon, located just upstream from the Durkee fault. Panel **C**. shows relief within the Burnt River catchment. Relief was calculated using a 100 m moving window with the focal range routine in ArcGIS. Similar to slopes, areas of high relief are isolated to the upper and lower Burnt River canyons. Elevation, slope, and relief were calculated from the 10 m resolution National Elevation Dataset.

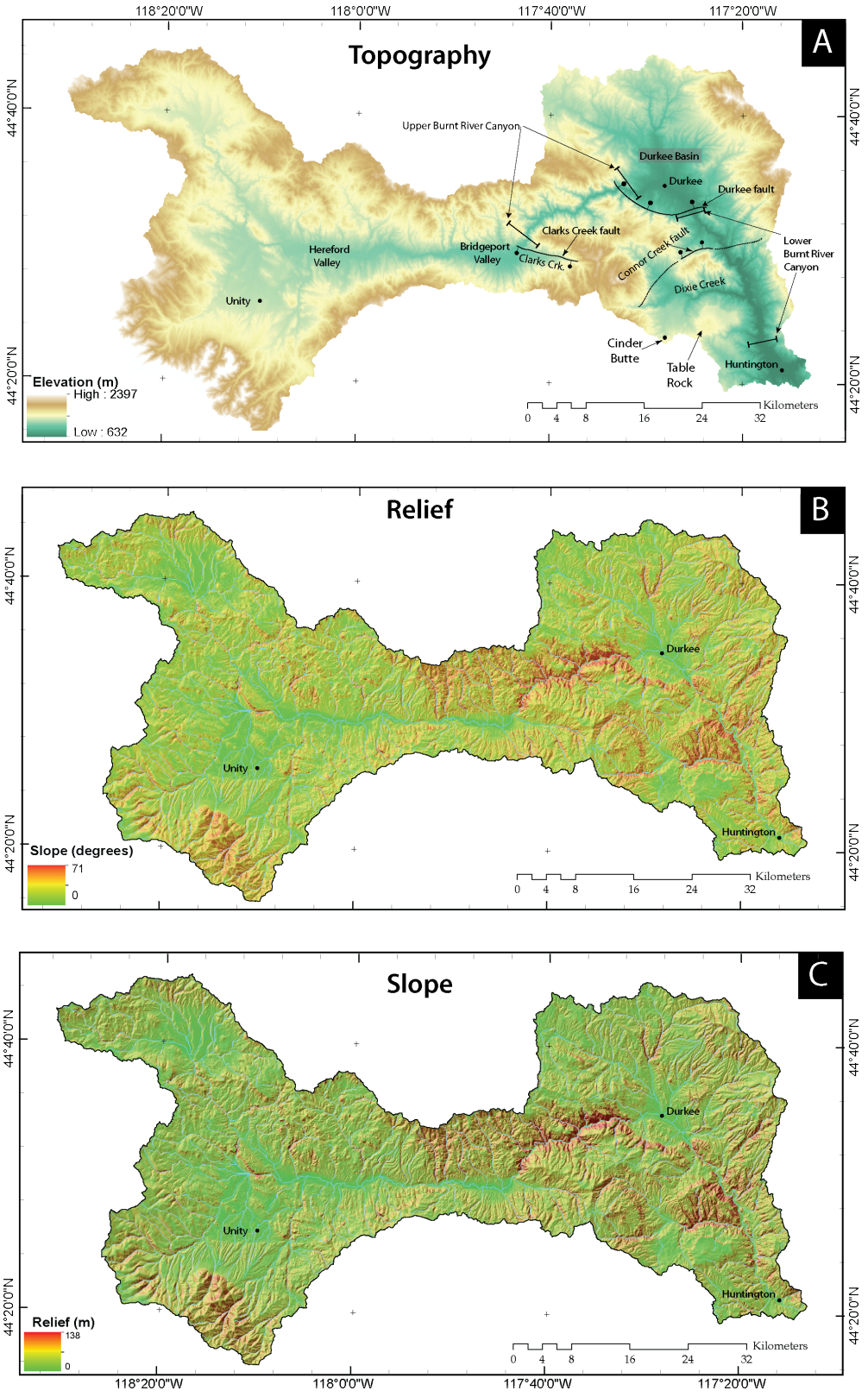
118°20'0"W
118°0'0"W
117°40'0"W
117°20'0"W
44°40'0"N
44°20'0"N
A
Topography
Upper Burnt River Canyon
Durkee Basin
Durkee
Durkee fault
Clarks Creek fault
Lower
Burnt River
Canyon
Hereford
Valley
Bridgeport
Valley
Clarks Crk.
Connor Creek fault
Dixie Creek
Unity
Cinder
Butte
Table
Rock
Huntington
Elevation (m)
High : 2397
Low : 632
0 4 8 16 24 32
Kilometers
B
Relief
Durkee
Unity
Huntington
Slope (degrees)
71
0
C
Slope
Relief (m)
138
0

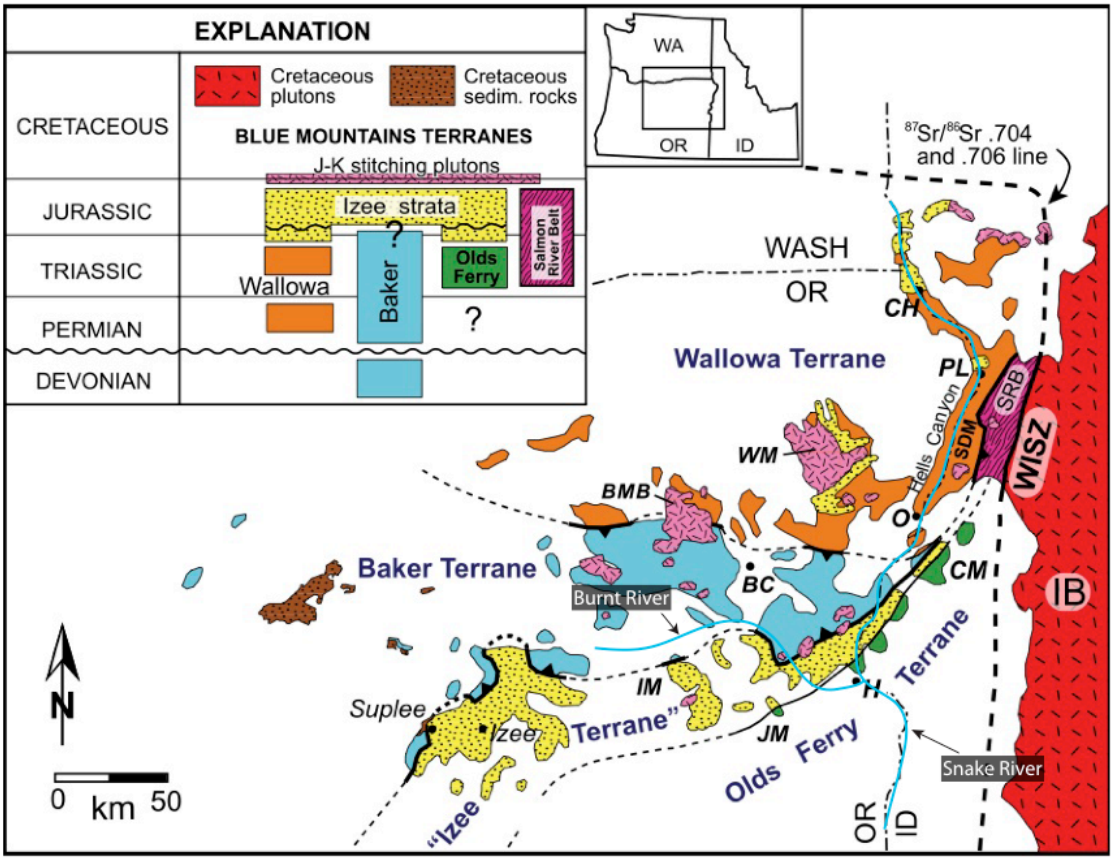

Figure 4. Paleozoic and Mesozoic accreted terranes exposed in eastern Oregon. BC – Baker City, BMB – Bald Mountain Batholith, H – Huntington, IB – Idaho Batholith, IM – Ironside Mountain, JM – Juniper Mountain, O – Oxbow, PL – Pittsburg Landing, CM – Cuddy Mountains, CH – Coon Hollow, SDM – Seven Devils Mountains, SRB – Salmon River belt, WM – Wallowa Mountains and batholith, WISZ – Western Idaho Shear/Suture Zone. The Burnt and Snake Rivers are overlain as blue lines (figure modified from Dorsey and Lamaskin, 2008).

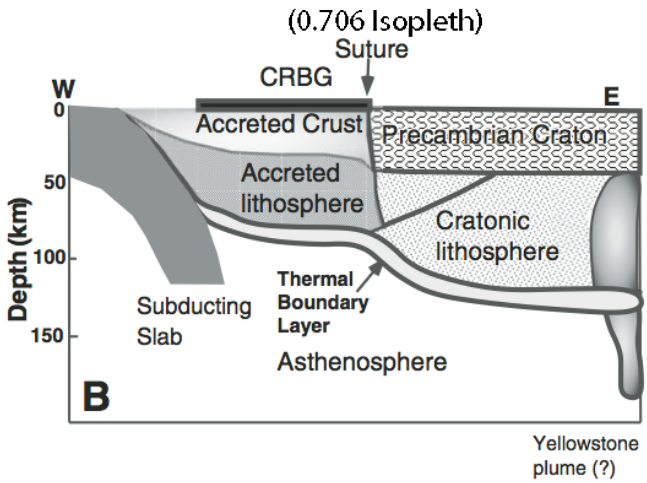

Figure 5. An east to west cross-section across the Sr 0.706 line and the Salmon River Suture zone. This image illustrates the present day difference in crustal thickness between mafic and juvenile accreted lithosphere and older, more felsic cratonic lithosphere. The initial pulse of the Yellowstone plume came into contact with the base of the North American lithosphere beneath the base of the accreted terranes, which Camp and Hanan (2008) invoked as a pathway for the northward propogation of the plume head. This image does not highlight the underplated Farallon lithosphere imaged by Darold and Humphreys (2013) (figure modified from Rodriguez and Sen, 2013).

Figure 6. Abbreviated Cenozoic geologic history of eastern Oregon that is important to the tectonic, volcanic, and dynamic development of Hells Canyon. For geographic reference to many of these events, see Figure 7. Ages are in millions of years. (Hooper and Swanson, 1990; Allen, 1991; Cummings et al., 2000; Wood and Clemens, 2002; Cowan and Reiners, 2004; Xue and Allen, 2006; Hooper, et al., 2007; Gaschnig et al., 2010; McClaughry et al., 2009; Gao et al., 2011; Schmandt and Humphreys, 2011; Streck et al., 2011; Reidel et al., 2013; Barry et al., 2013; Ferns and McClaughry, 2013; Nicolaysen et al., 2014)

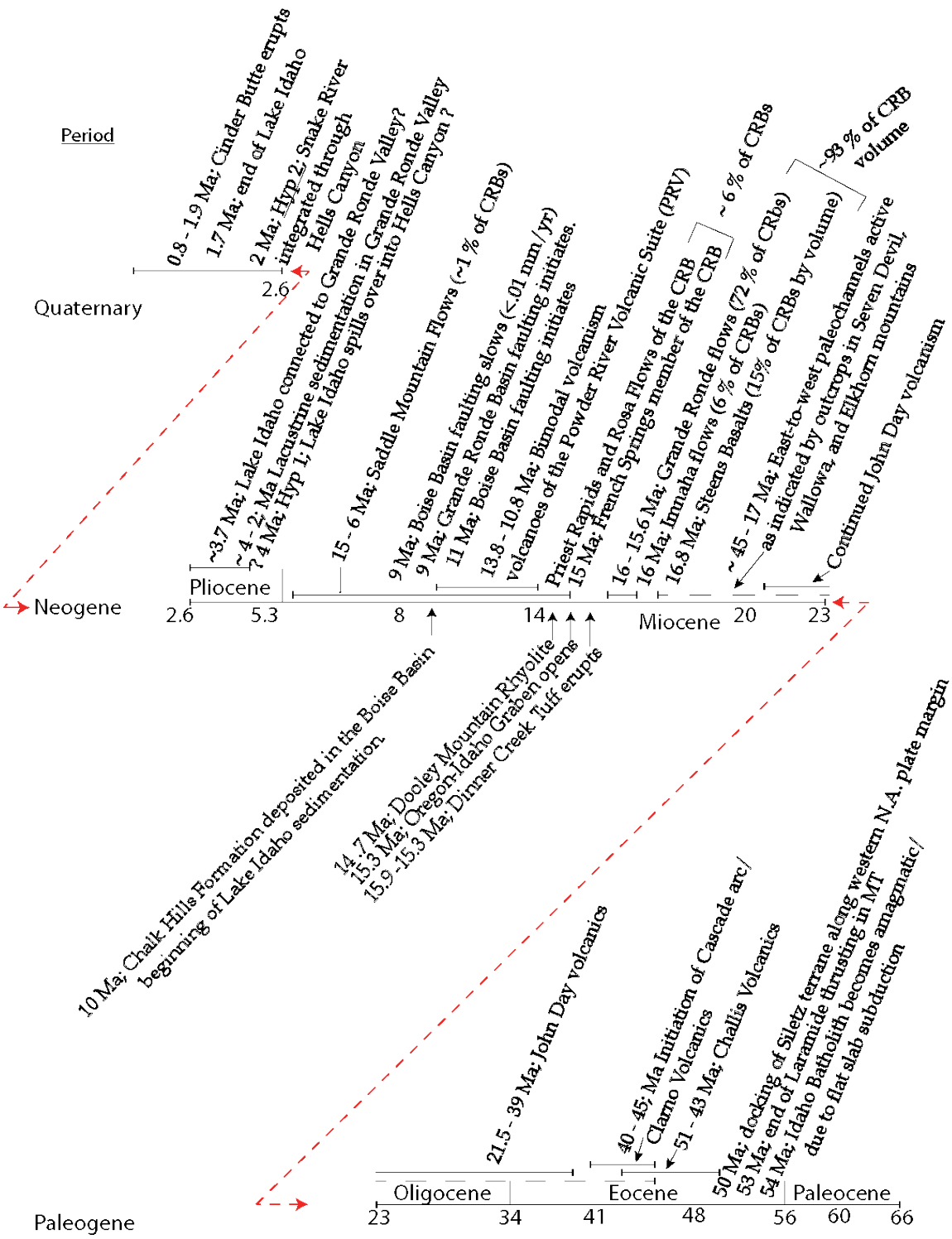
Period
Quaternary
Neogene
Paleogene
2.6
Pliocene
5.3
8
14
Miocene
20
23
Oligocene
34
41
48
Eocene
56
60
66
Paleocene
0.8 - 1.9 Ma; Cinder Butte erupts
1.7 Ma; end of Lake Idaho
2 Ma; Hyp 2; Snake River integrated through Hells Canyon
~3.7 Ma; Lake Idaho connected to Grande Ronde Valley?
~ 4 - 2; Ma Lacustrine sedimentation in Grande Ronde Valley
? 4 Ma; Hyp 1; Lake Idaho spills over into Hells Canyon ?
15 - 6 Ma; Saddle Mountain Flows (~1 % of CRBs)
9 Ma; Boise Basin faulting slows (<.01 mm/yr)
9 Ma; Grande Ronde Basin faulting initiates.
11 Ma; Boise Basin faulting initiates
13.8 - 10.8 Ma; Bimodal volcanism
volcanoes of the Powder River Volcanic Suite (PRV)
Priest Rapids and Rosa Flows of the CRB
15 Ma; French Springs member of the CRB
16 - 15.6 Ma; Grande Ronde flows (72 % of CRBs)
16 Ma; Imnaha flows (6 % of CRBs)
16.8 Ma; Steens Basalts (15% of CRBs by volume)
~ 6 % of CRBs
~93 % of CRB volume
~ 45 - 17 Ma; East-to-west paleochannels active as indicated by outcrops in Seven Devil, Wallowa, and Elkhorn mountains
Continued John Day volcanism
10 Ma; Chalk Hills Formation deposited in the Boise Basin beginning of Lake Idaho sedimentation.
14.7 Ma; Dooley Mountain Rhyolite
15.3 Ma; Oregon-Idaho Graben opens
15.9 -15.3 Ma; Dinner Creek Tuff erupts
21.5 - 39 Ma; John Day volcanics
40 - 45; Ma Initiation of Cascade arc/ Clarno Volcanics
51 - 43 Ma; Challis Volcanics
50 Ma; docking of Siletz terrane along western N.A. plate margin
53 Ma; end of Laramide thrusting in MT
54 Ma; Idaho Batholith becomes anagmatic/ due to flat slab subduction

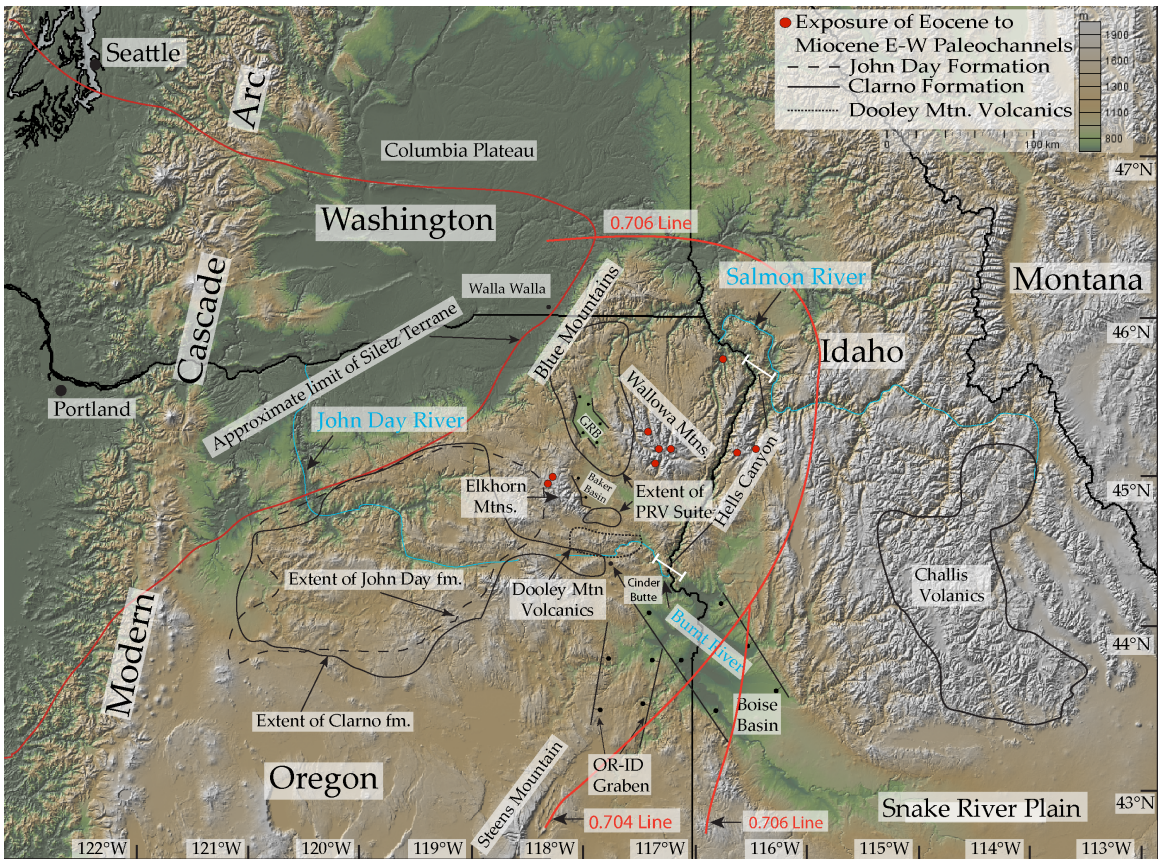

Figure 7. Extent of major Cenozoic volcanic, tectonic, and depositional episodes in eastern Oregon and western Idaho. For ages and references see Figure 6. Elevations for this figure were derived from the 30 m resolution National Elevation Dataset, using the GeoMapApp.

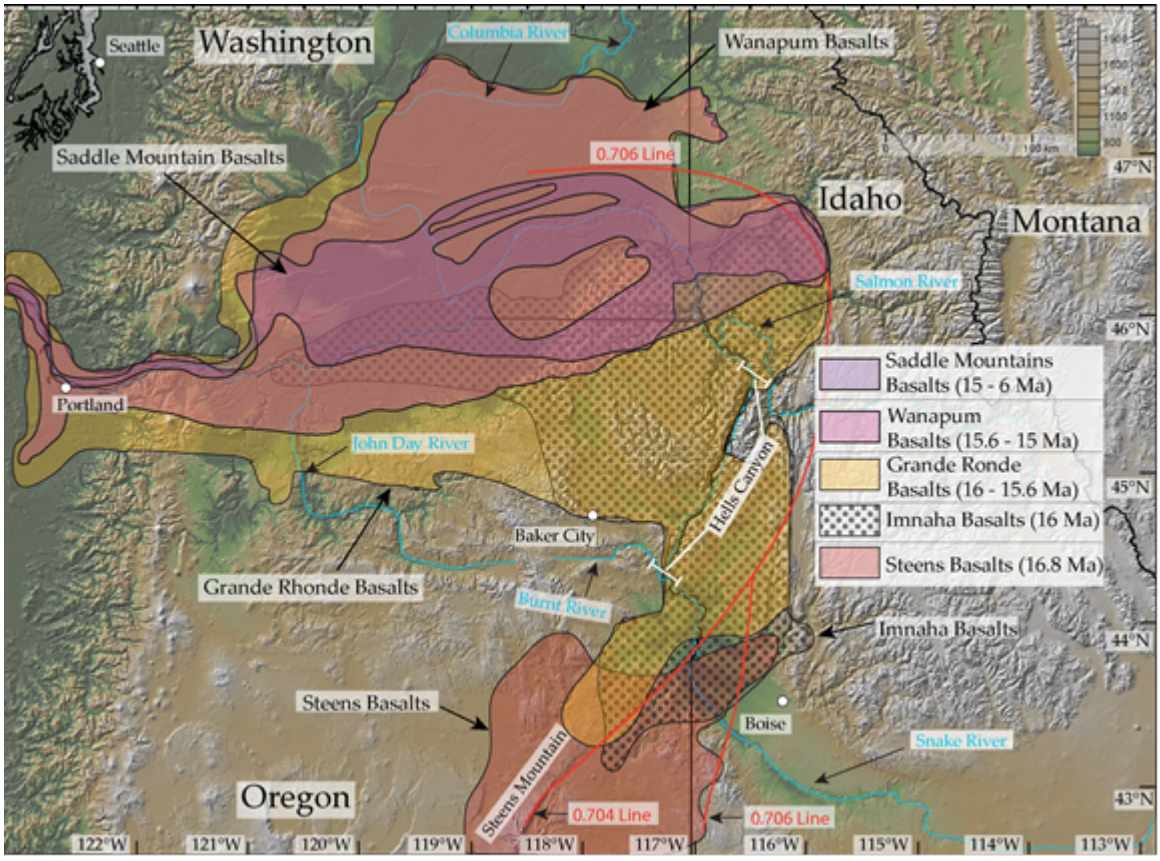

Figure 8. Aerial extent of the Steens and Columbia River Basalts. Note the northward migration of flows with time, starting with the eruption of the Steens Basalts at ~16.8 Ma at the Idaho-Oregon-Nevada triple point. The eruptive volume of the Columbia River Basalts peaked with the initial Imnaha flows and subsequent Grande Ronde Basalts. The basalts roughly track the edge of cratonic North America ($^{87}Sr/^{86}Sr$ 0.706 isopleth), likely exploiting existing weaknesses in the thinner accreted lithosphere (e.g. Camp and Hanan, 2008; Pierce and Morgan, 2009; Reidel et al., 2013; Reidel and Tolan, 2013a).

Figure 9. The two competing hypotheses for Yellowstone plume interactions with North America that both yield lithospheric delamination and the different Columbia River Basalt flows. **Left (A):** The Darold and Humphreys (2013) model which presents plume-aided delamination of underplated Farallon lithosphere and detachment of an ultramafic root below the Wallowa Mountains. Panels A1 – A4 are time progressive from initial plume contact (A1) to the initial rollback of Farallon lithosphere (A2) and onto destabilization of the ultramafic roof of the Wallowa batholith (A3). The slab rollback pulls the plume head to the north, explaining the northward progression of basalts with time. All of these events combine to produce modern topography in eastern Oregon; a "bull's eye" shaped mountain range with the Wallowa Mountains at its center and flanking extensional basins, including the Durkee Basin. **Right (B):** The Camp and Hanan (2008) hypothesis for plume-lithosphere interactions. As the plume travels along the base of the thinner, accreted lithosphere, it flows "uphill" to the north. Plume asthenosphere interacts with the thinner and weaker lithosphere of the accreted terranes leads to instabilities that detach and sink into the asthenosphere (B1 –B2). Hot plume asthenosphere exploits these weaknesses, generating the melt associated with the Steens and Columbia River Basalts (figures modified from Camp and Hanan, 2008; Darold and Humphreys, 2013).

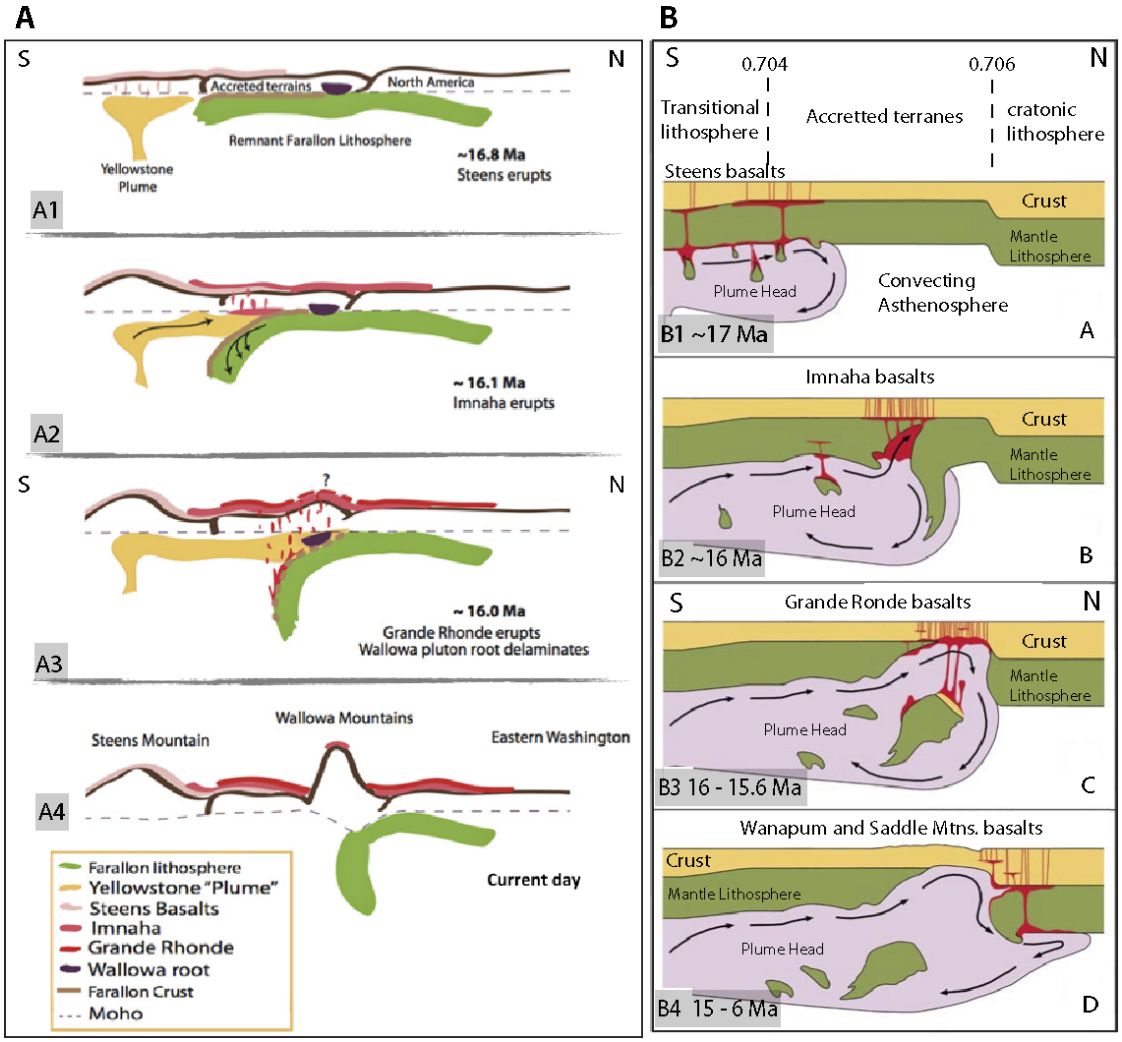
A
S
N
Accreted terrains
North America
Remnant Farallon Lithosphere
Yellowstone Plume
~16.8 Ma
Steens erupts
A1
~ 16.1 Ma
Imnaha erupts
A2
S
N
?
~ 16.0 Ma
Grande Rhonde erupts
Wallowa pluton root delaminates
A3
Wallowa Mountains
Steens Mountain
Eastern Washington
A4
Current day
Farallon lithosphere
Yellowstone "Plume"
Steens Basalts
Imnaha
Grande Rhonde
Wallowa root
Farallon Crust
Moho
B
S
0.704
0.706
N
Transitional lithosphere
Accretted terranes
cratonic lithosphere
Steens basalts
Crust
Mantle Lithosphere
Plume Head
Convecting Asthenosphere
B1 ~17 Ma
A
Imnaha basalts
Crust
Mantle Lithosphere
Plume Head
B2 ~16 Ma
B
S
Grande Ronde basalts
N
Crust
Mantle Lithosphere
Plume Head
B3 16 - 15.6 Ma
C
Wanapum and Saddle Mtns. basalts
Crust
Mantle Lithosphere
Plume Head
B4 15 - 6 Ma
D

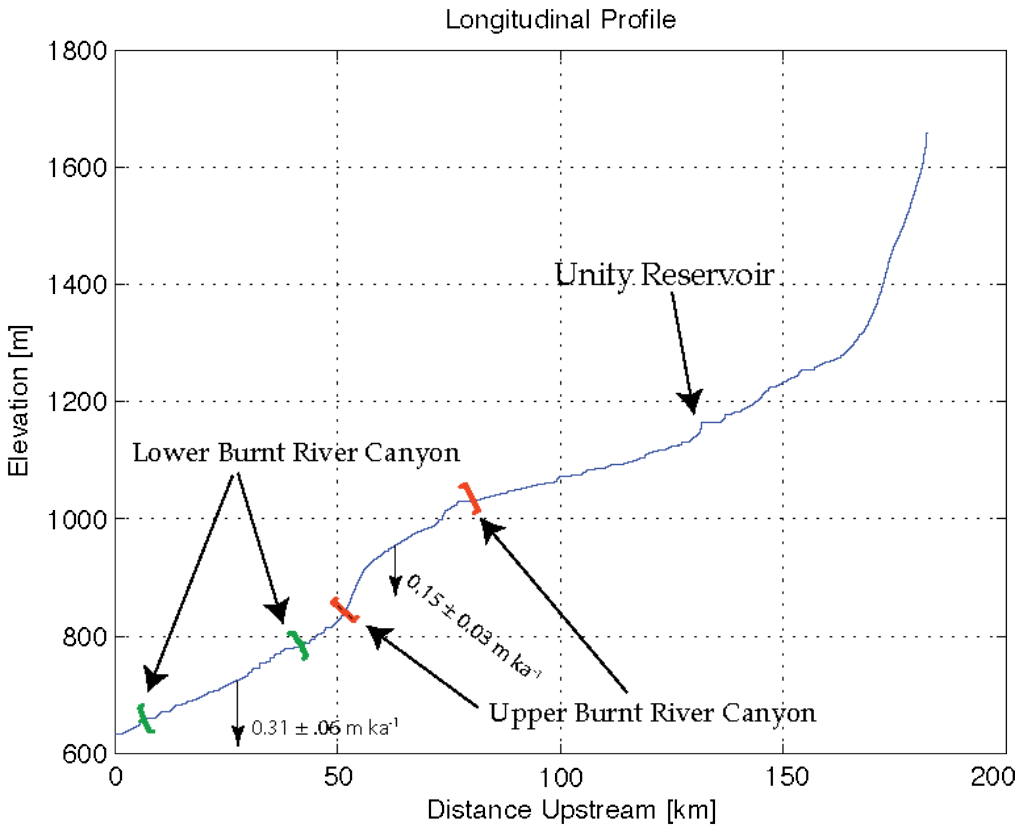

Figure 10. Longitudinal profile of the Burnt River from its confluence with the Snake River (Brownlee Reservoir) to its headwaters. The upper Burnt River canyon is notable as the river steepens significantly in this reach. The lower Burnt River canyon exhibits a straight, yet consistently steep gradient. Both the lower and upper Burnt River canyons are steeper than the section of river just above the upper canyon. The fluvial incision rates for the upper and lower Burnt River canyons are presented in Table 4. This longitudinal profile was extracted using the MATLAB native TopoToolbox 2 script (Schwanghart and Scherler, 2014).

Figure 11. Field photos of landforms mapped in the upper and lower Burnt River canyons. (**A**) Terrace deposits consisting of imbricated cobbles overlain by colluvial debris and a soil. This section is exposed in a large hydraulic mining cut in the upper Burnt River canyon. (**B**) Boulder-sized clasts exhumed by hydraulic mining activities were observed in several of the terrace deposits. (**C**) Large stretches of mining-disturbed alluvium was mapped as Quaternary Modified Land (Qml). Dredging operations moved large quantities of alluvium from the Burnt River and surrounding hillslopes. (**D**) Quaternary travertine deposits crop out along with active springs along the line of the recently mapped Durkee fault. (**E**) A terrace as seen from the upper Burnt River Canyon Road. Mining operations exposed the strath (not visible), tread, and colluvial cover that are now in excess of 100 m above the modern river. (**F**) Several landslides were mapped in the upper and lower Burnt River canyon. This shallow earthflow is located in the upper Burnt River canyon.

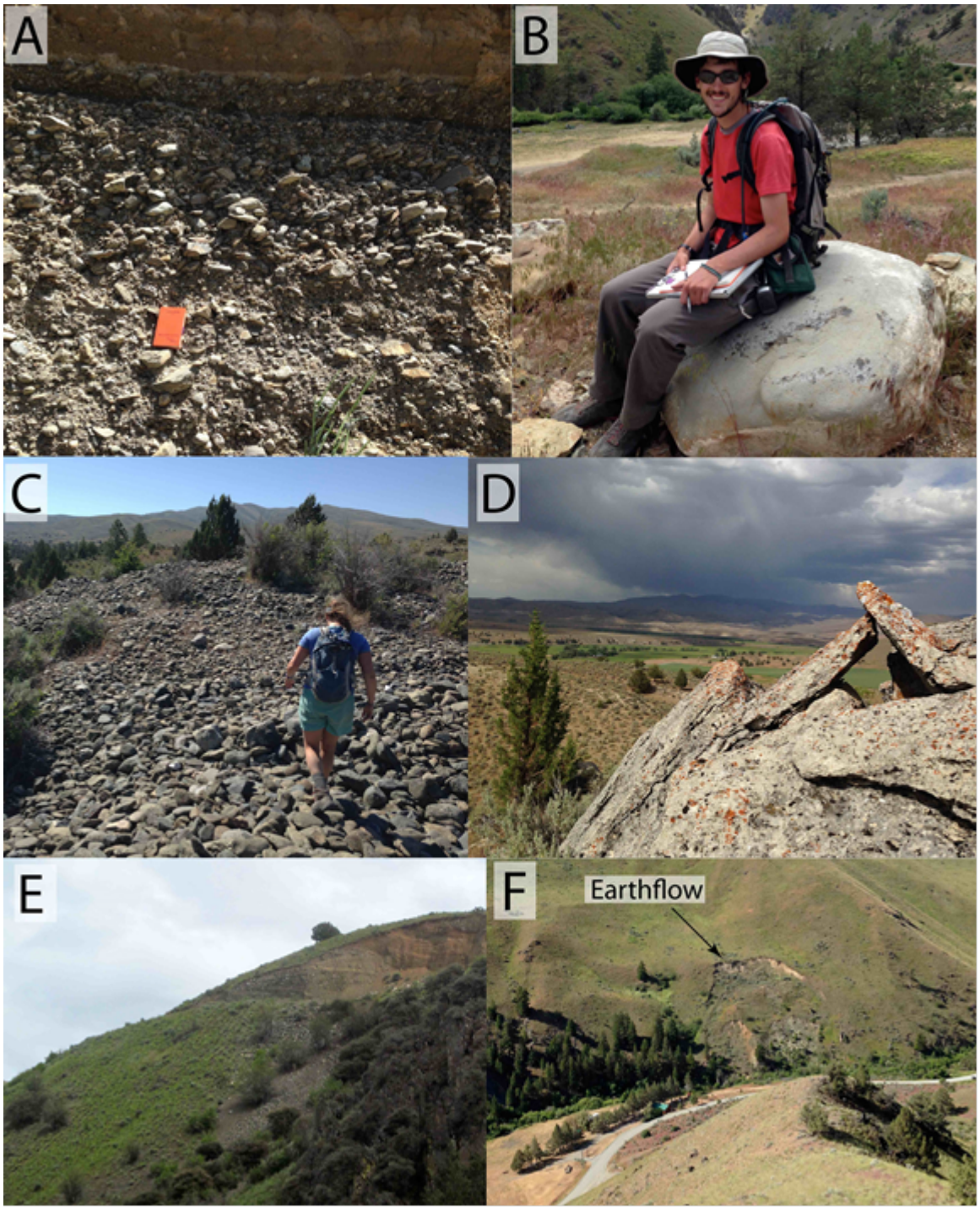
A
B
C
D
E
F
Earthflow

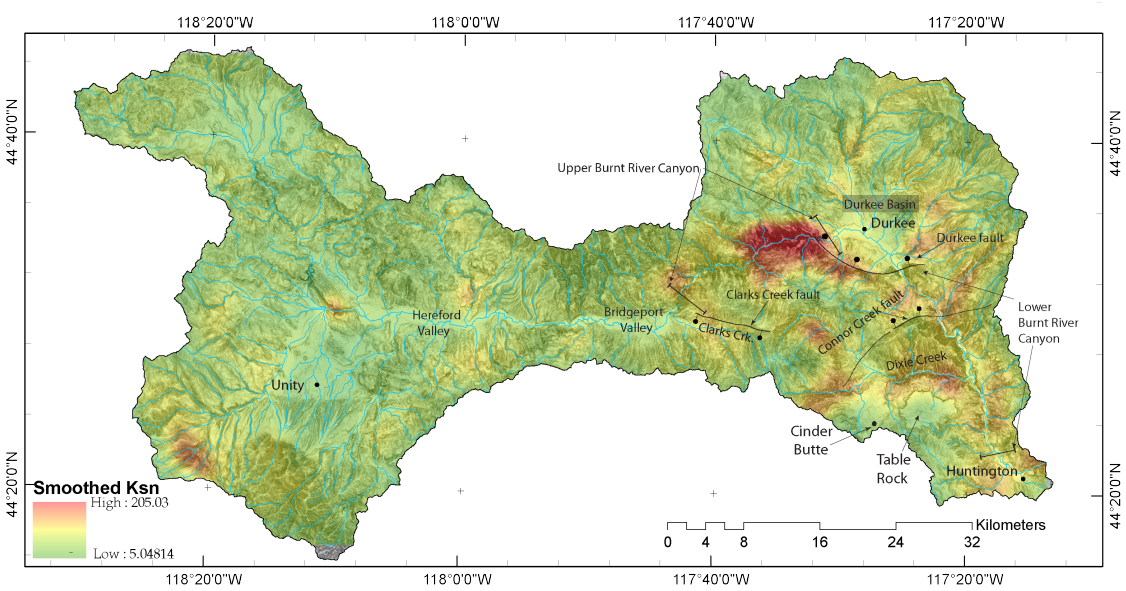

Figure 12. Normalized channel steepness (*Ksn*) for the Burnt River catchment. Values were smoothed using a 100 m moving window following the method outlined in Miller et al. (2013). Warmer colors represent areas in which streams are steeper (normalized for drainage area). The "hot spot" of steeper channels coincident with the upper Burnt River canyon is likely due to the presence of the previously unmapped Durkee fault at the mouth of the canyon, providing a first-order control on local base level. The Burnt River catchment downstream from the Durkee Basin still contains steeper streams than exits in the upper half of the catchment, indicating that the Durkee fault is not the only control on fluvial channel evolution in the basin. Stream steepnesses was calculated using the MATLAB-based TopoToolbox (Schwanghart and Scherler, 2014).

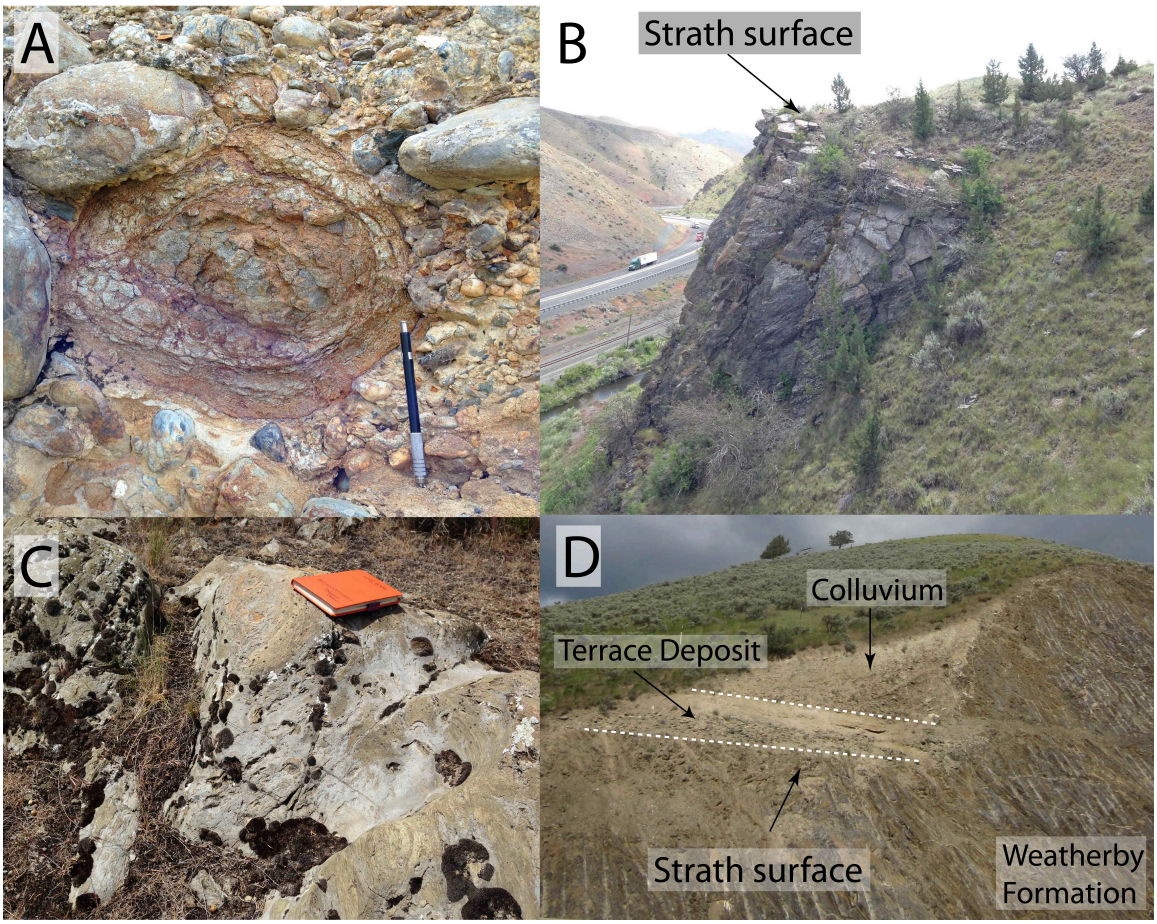

Figure 13. Terrace deposit photos. (**A**) Basalt weathering rinds provided a relative chronometer of terrace age in the lower Burnt River canyon. (**B**) Hydraulic gold mining often removed all terrace deposits and colluvial cover, leaving the strath surface exposed. The apparent tilt of the strath surface is due to the dip of the underlying limestone units. (**C**) Erosional potholes bored into the bedrock strath are an indication of the former fluvial nature of the surface. This photo is a close up of the terrace in (**B**). (**D**) Several I-84 road cuts expose strath surfaces, terrace deposits and colluvial cover, as depicted in this photograph near milepost 336.

Figure 14. A tephra deposit in the tread of the $Qt5_U$ terrace in the upper Burnt River canyon was identified by staff at the WSU tephrochronology laboratory as the ~ 160 Ka Paoha Island tephra from Mono Lake, California. Subsequent research indicates that the Paoha Island tephra is actually 201 ± 47 ka (Kuehn and Negrini, 2010). (**A**) The tephra is interbedded with fine-grained fluvial over bank deposits atop coarser, axial-channel gravels. (**B**) This $Qt5_U$ terrace was identified in a mining cut, ~5 m above the Qt5 strath and ~12 m above the $Qt6_U$ strath (both identified by the dashed red lines).

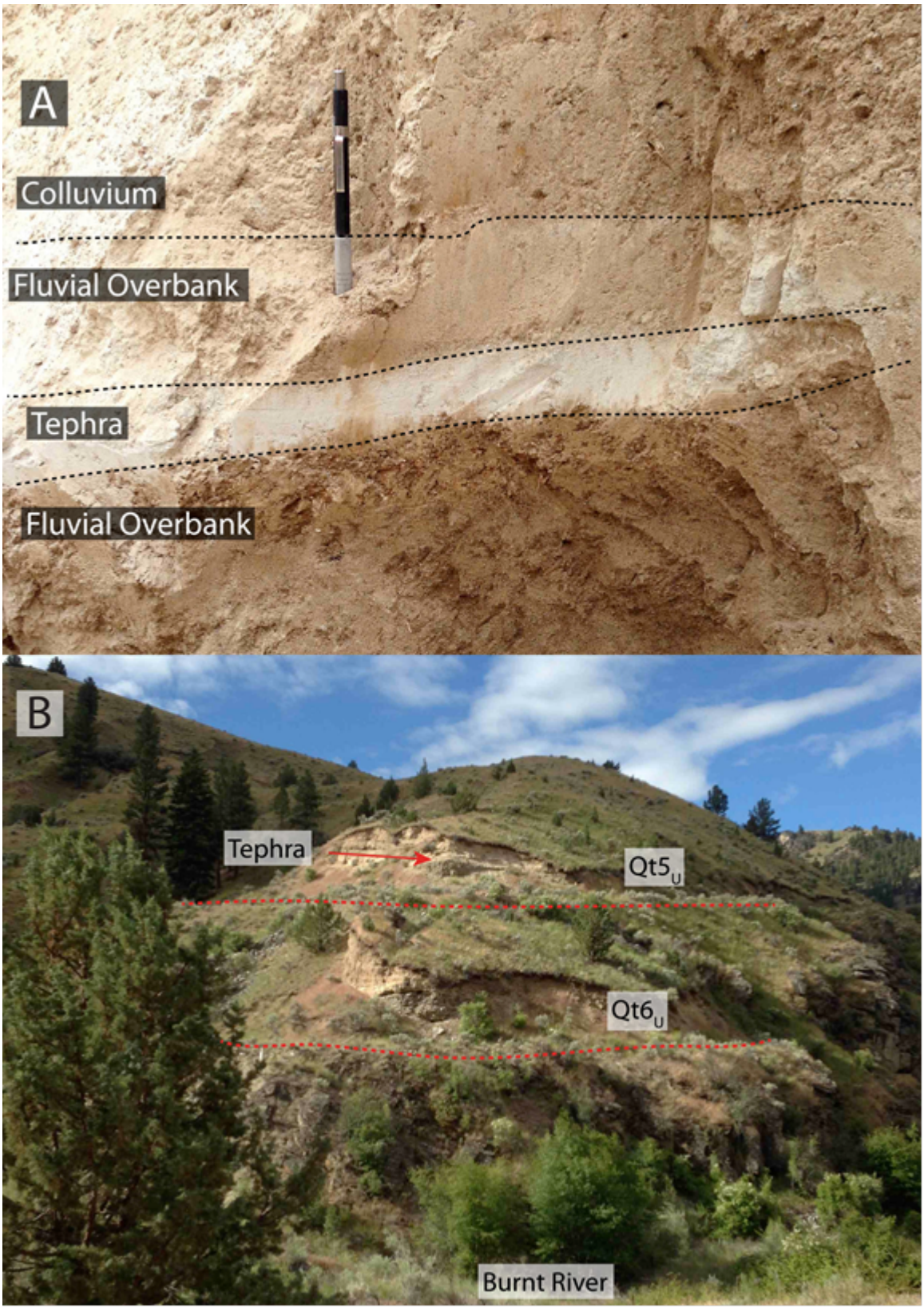
A
Colluvium
Fluvial Overbank
Tephra
Fluvial Overbank
B
Tephra
Qt5U
Qt6U
Burnt River

Figure 15. Optically Stimulated Luminescence (OSL) sample collection. (**A**) Samples were gathered from fine-grained beds within terrace gravels. These finer grained units were often flood overbank silts and sands. Terrace gravels are at the bottom of the image with several finer grained beds next to and above the scale card. The sample was collected in the recessed bed, which contained fine-grained quartz-rich sand. (**B**) Following the Utah State University OSL sampling procedure, samples were collected using steel pipe (at least 20 cm long) and sealed with both Styrofoam and duct-tape. (**C**) OSL sample pipe in the outcrop before removal (Styrofoam is visible). Sample was taken from fine-grained deposit atop terrace gravels.

Figure 16. Topographic metrics for tributary catchments along the length of the Burnt River, including normalized hypsometry, mean slope, normalized elevation, and hypsometric integral (*HI*) for tributary catchments along the length of the Burnt River. Plots illustrate different levels of landscape adjustment to a transient signal and tectonic activity. Hypsometry and hypsometric integral calculations indicate catchments likely in equilibrium (1 and 2) and catchments in disequilibrium (3 – 7). Elevation and slope plots help to identify high elevation areas of low-slope that have not yet adjusted to stream incision driven by either local or regional base level changes.

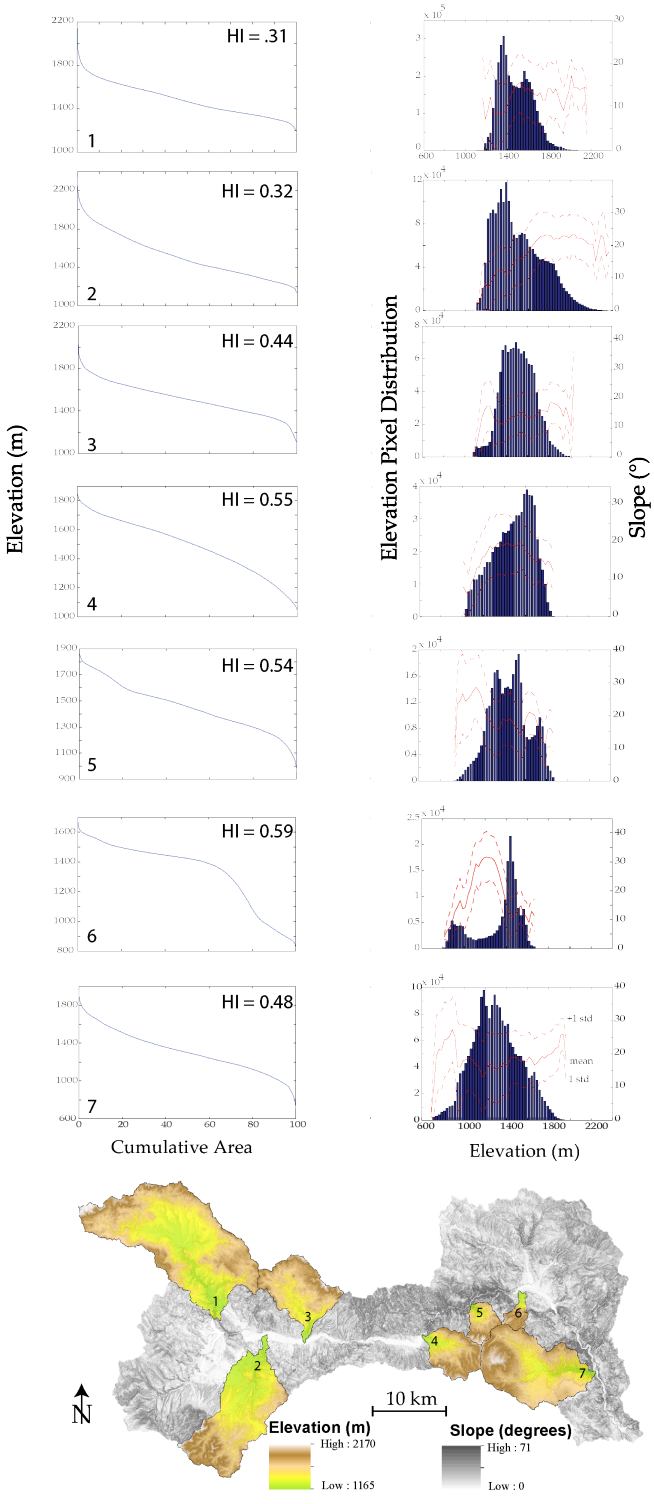
HI = .31
1
HI = 0.32
2
HI = 0.44
3
HI = 0.55
4
HI = 0.54
5
HI = 0.59
6
HI = 0.48
7
Elevation (m)
Cumulative Area
Elevation Pixel Distribution
Slope (°)
Elevation (m)
+1 std
mean
-1 std
N
10 km
Elevation (m)
High : 2170
Low : 1165
Slope (degrees)
High : 71
Low : 0

Figure 17. Correlations between Burnt River terraces in the upper (**A**) and lower canyons (**B**). The solid black line is the longitudinal profile extracted from the 10 m resolution National Elevation Dataset that was smoothed in SigmaPlot using a 1st-order polynomial LOESS tricube weighting routine with a kernel 0.1 times the river length in order to remove artificial steps from the digital elevation dataset. Terrace locations are plotted using elevation data from differential GPS field measurements. The spatial location of different geologic units are denoted on the map-view of the Burnt River channel planform shown above the longitudinal profiles for both the upper and lower canyons, respectively.

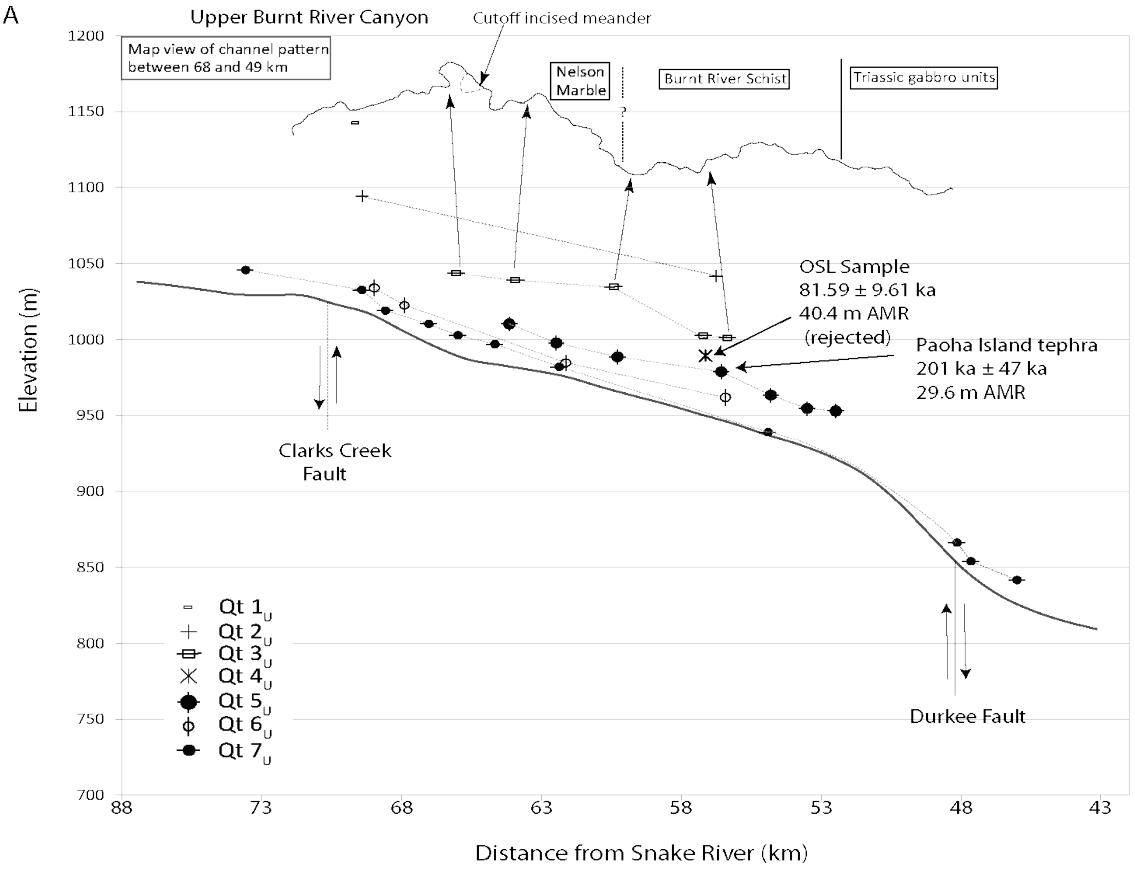
A
Upper Burnt River Canyon
Cutoff incised meander
Map view of channel pattern between 68 and 49 km
Nelson Marble
Burnt River Schist
Triassic gabbro units
OSL Sample
81.59 ± 9.61 ka
40.4 m AMR
(rejected)
Paoha Island tephra
201 ka ± 47 ka
29.6 m AMR
Clarks Creek Fault
Durkee Fault
Qt 1U
Qt 2U
Qt 3U
Qt 4U
Qt 5U
Qt 6U
Qt 7U
Elevation (m)
Distance from Snake River (km)

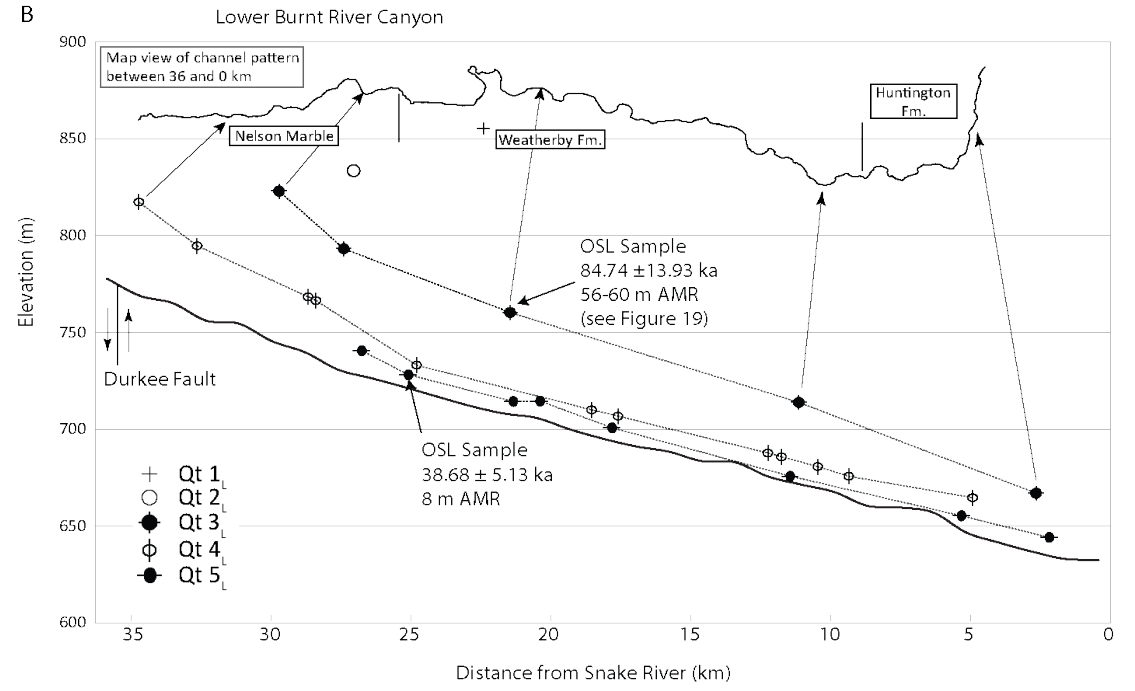
B
Lower Burnt River Canyon
Map view of channel pattern between 36 and 0 km
Nelson Marble
Weatherby Fm.
Huntington Fm.
OSL Sample
84.74 ±13.93 ka
56-60 m AMR
(see Figure 19)
Durkee Fault
OSL Sample
38.68 ± 5.13 ka
8 m AMR
Qt 1L
Qt 2L
Qt 3L
Qt 4L
Qt 5L
Elevation (m)
Distance from Snake River (km)

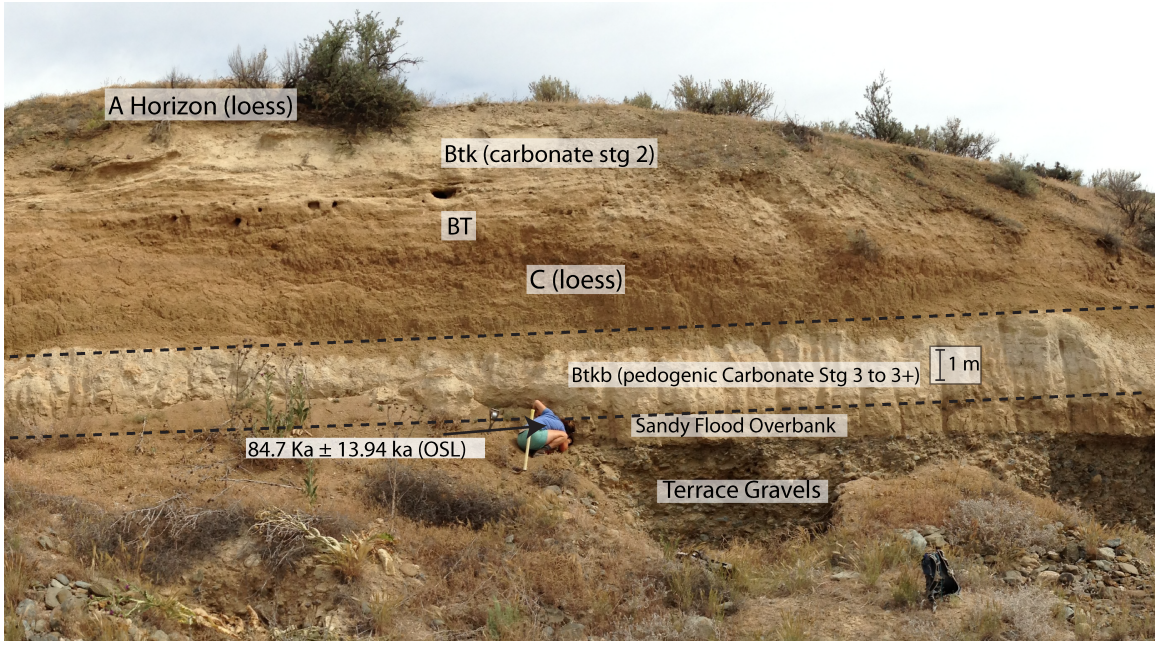

Figure 18. An outcrop of the $Qt3_L$ terrace in the lower Burnt River canyon that contains two distinct soils above terrace gravels [location: N 44.4731°, W 117.3336°]. Post-gravel stratigraphy represents two episodes of loess accumulation and soil development. The lower 3 to 3+ soil carbonate (Btkb) horizon likely correlates to the Btk horizon of the Devils Canyon Soil (MIS 4, ~60 to 70 ka) in the Palouse Hills; while the upper Btk soil carbonate horizon correlates to the Btk horizon of the Washtucna Soil (MIS 2, ~24 ka) in the Palouse soil chronostratigraphy (McDonald et al., 2012). The degree of soil development observed at this exposure is consistent with the acquired OSL age of 84.7 ± 13.94 ka obtained from the flood over bank deposits just below the Btkb horizon.

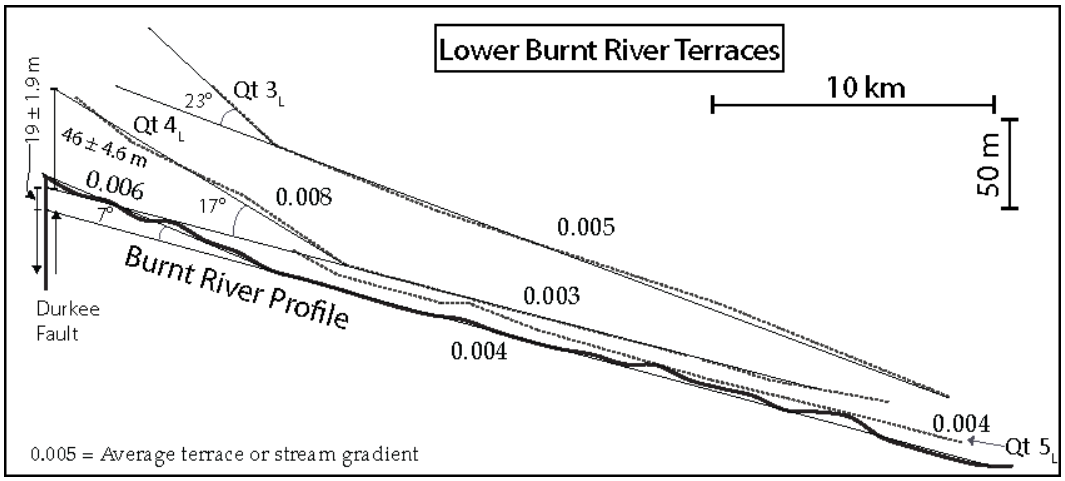

Figure 19. Terrace and modern channel gradients for the lower Burnt River canyon. Terraces proximal to the Durkee fault are over-steepened with respect to downstream counterparts. The deformed segment of the $Qt4_L$ terrace is ~ 46 m higher at the fault plane than the projection of the undeformed section of the same terrace. This deformation indicates that the $Qt4_L$ terraces have been over steepened by accumulated throw on the Durkee fault. Additionally, the upper 10 km of the modern Burn River is ~ 19 m higher at the Durkee fault plane than it would be if it maintained the same gradient as the downstream section. This deflection may be due to a rock type change from the harder Nelson Marble into the more erodible Weatherby Formation. Additionally, the Burnt River likely loses stream power and cutting tools as it travels across the Durkee Basin, two suggestions that are inconsistent with the steeper terrace and channel gradients immediately downstream from the fault. See Table 5 for gradient data.

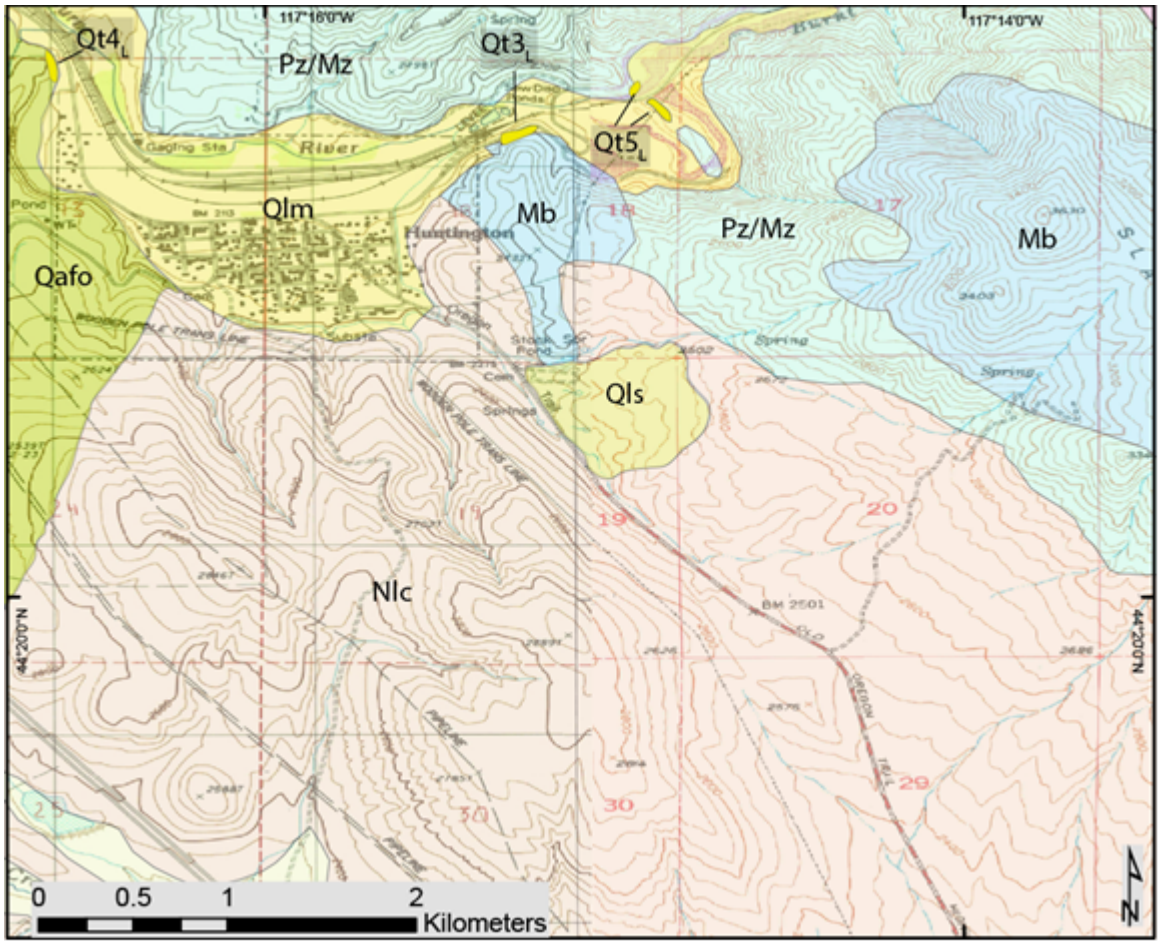

Figure 20. Geologic Map of the Huntington, Oregon area overlain on the 7.5-minute U.S.G.S. Huntington and Olds Ferry topographic quadrangle maps. Elevations are in feet with 40 foot contour intervals. Pz/Mz – Paleozoic and Mesozoic Huntington Formation (Brooks, 1979a). Mb – Miocene basalt flows, likely Grande Ronde and Imnaha flows. Nlc – Neogene lacustrine units. These lake beds are likely part of the Miocene to Pliocene Lake Idaho sediments mapped in the adjacent Boise Basin (Wood and Clemens, 2002). Qafo – Quaternary alluvial fan (old). This unit is composed almost exclusively of basalt cobbles. Modern streams have incised through this alluvial fan. This fan may have formed in a wetter climate. Qls – Quaternary landslide. At the time of mapping, this was an active earthflow that had recently damaged US Route 30 to the point where the Oregon Department of Transportation no longer paves this portion of the highway. Qlm – Quaternary modified land. This unit has been mapped in the past by Brooks (1979a, b) as Quaternary Alluvium. However, due to visible disturbance by late 19th and early 20th century gold mining activity, including the dredging and rerouting of the Burnt River, almost the entire fluvial system has been modified from its pre-mining form. Qt(3,4, 5$_L$) newly mapped Quaternary terraces with designations matching Figure 17B.

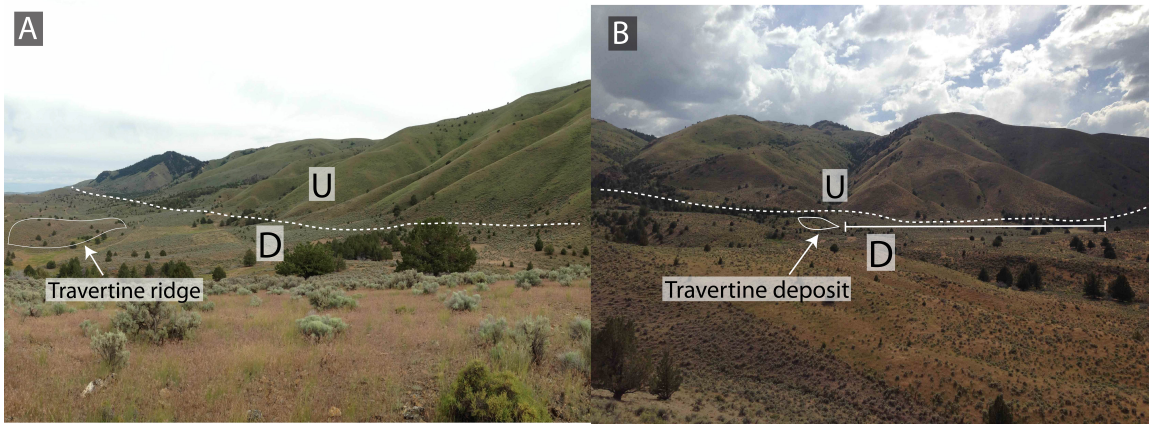

Figure 21. Two perspective views of the Durkee fault. (**A**) View to the south-southeast across the mountain front defined by the Durkee fault. An elongate outcrop of travertine now forms a ridge on the hanging wall side of the fault (photographed from N 44.571947°, W 117.529318°). The fluids that deposited the travertine flowed through a paleochannel, likely draining the mountain front. With time and preferential erosion of less-resistant late Miocene-to-Pliocene lacustrine sediments, the former paleo-low is now a high-standing ridge. (**B**) View southwest towards the mountain frontfrom the Durkee basin (photographed from N 44.570550°, W 117.507719°). The solid line just above the letter "D" identifies one of the prominent mountain front triangular facets. The presence of first order drainages cut into the face of this triangular facet may relate to slow movement along the Durkee fault or lack of recent activity. Another travertine deposit was mapped at the mouth of the drainage in the center of (**B**).

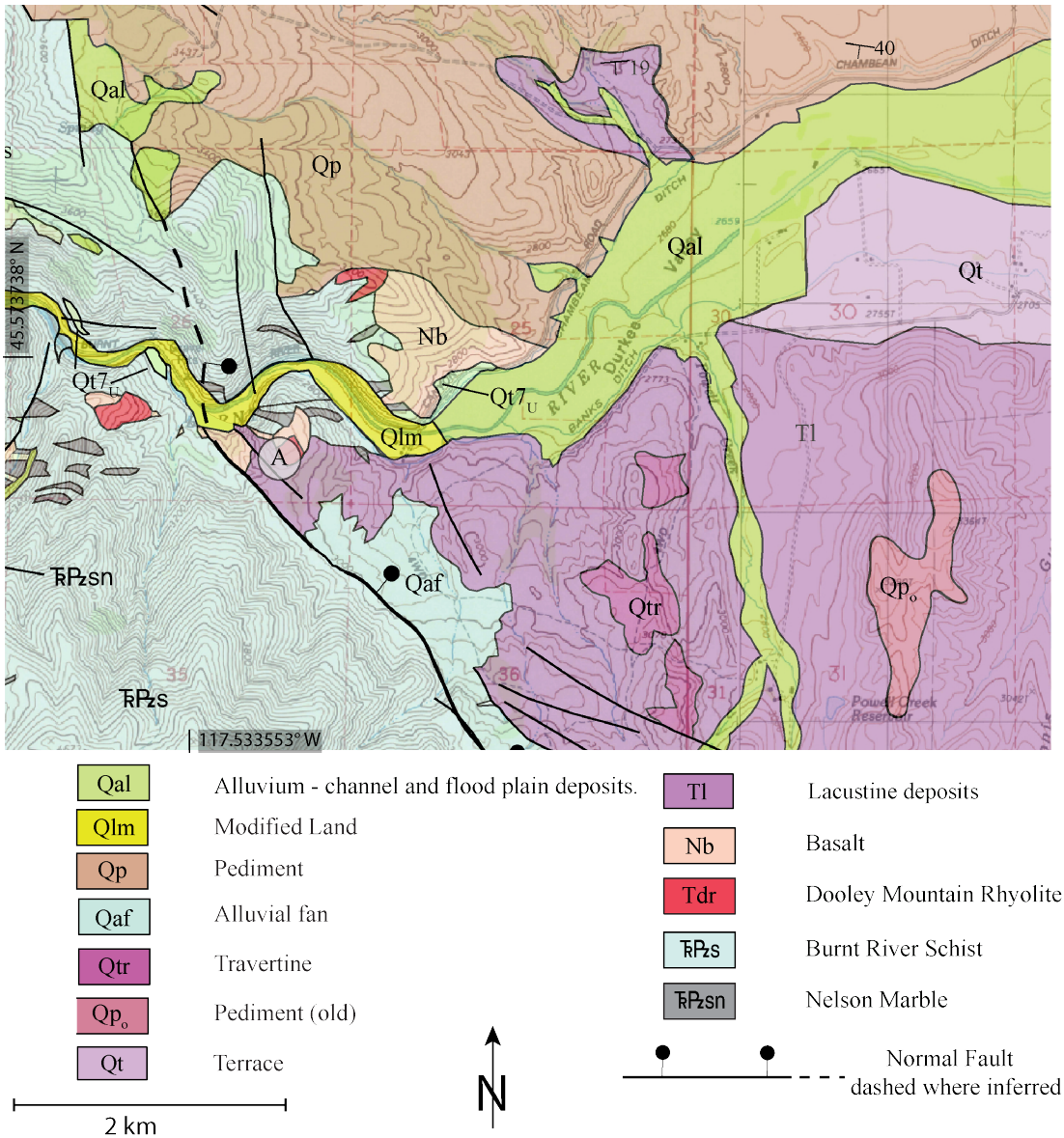

Figure 22. Geologic map of western edge of the Durkee Basin and lower three kilometers of the upper Burnt River canyon. Miocene to Pliocene lacustrine units are eroded into a pediment surface, and cut again by modern channels. A ridge of travertine marks a paleo-channel that now occurs stands as a topographic high due to differential erosion of the underlying lacustrine units. Location "A" references a photo found in Appendix – C.

Figure 23. (**A**) Hillshade image of the Durkee Basin with the location of a 10 km wide topographic swath profile that parallels the Durkee fault. The hillshade was constructed using the 10 m resolution National Elevation Dataset and tools native to ArcGIS. (**B**) Topographic swath data, showing minimum, mean, and maximum elevations along the 10 km wide section. The dashed line represents maximum elevations, a proxy for displacement along the Durkee fault, indicating a total footwall displacement of at least 0.5 km (indicated by the black vertical arrow). The red line is the approximate location of the Durkee fault, with a length of 16 km. The ratio between maximum displacement (D_{max}) and fault length (L) is 0.031. Abbreviations include: TBG – True Blue Gulch; PC – Powell Creek; HC – Hollowfield Canyon; GH – Gold Hill.

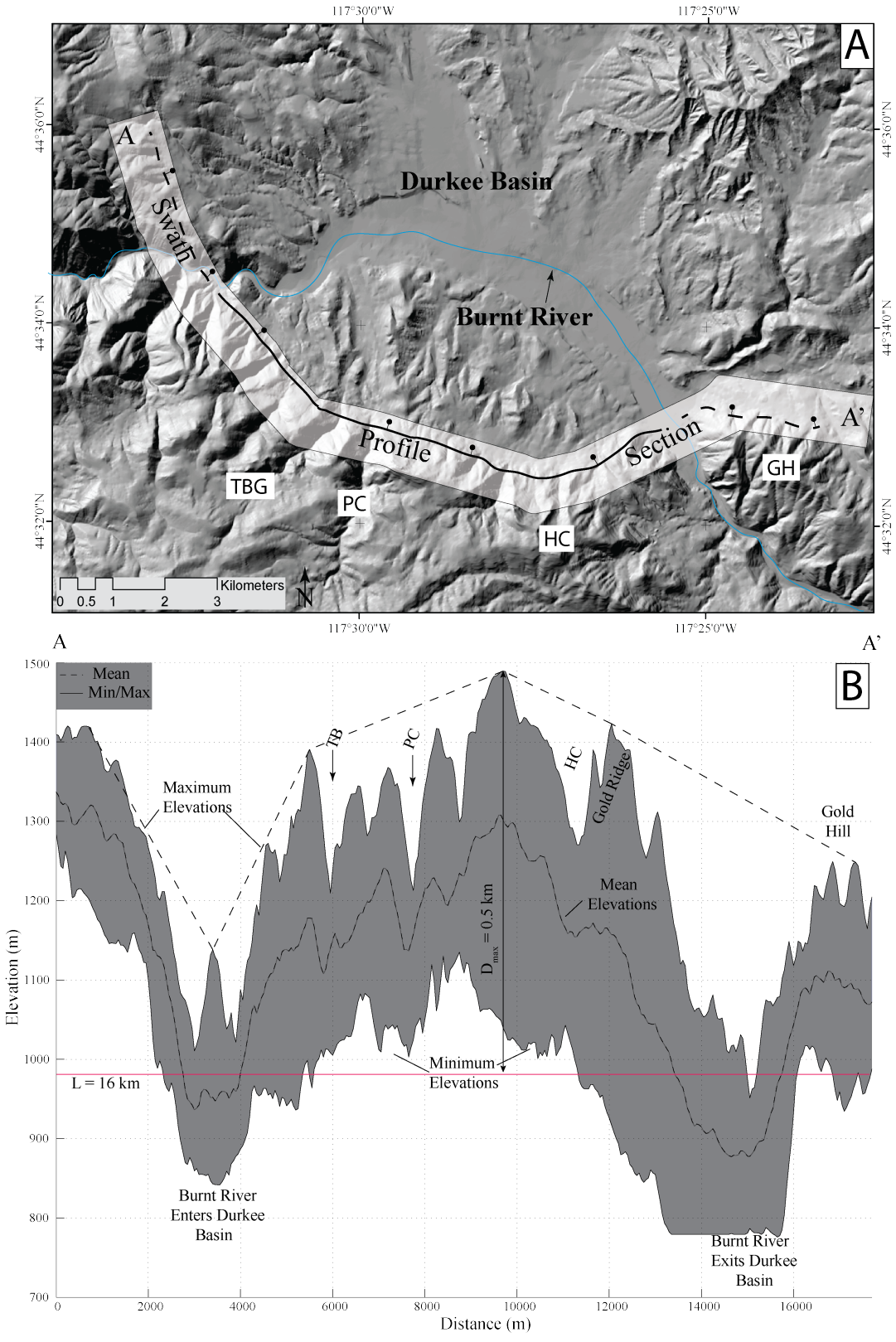
A
117°30'0"W
117°25'0"W
44°36'0"N
44°34'0"N
44°32'0"N
Durkee Basin
Burnt River
A
A'
Swath
Profile
Section
TBG
PC
HC
GH
Kilometers
0 0.5 1 2 3
N
B
Mean
Min/Max
Maximum Elevations
Mean Elevations
Minimum Elevations
TB
PC
HC
Gold Ridge
Gold Hill
D_{max} = 0.5 km
L = 16 km
Burnt River Enters Durkee Basin
Burnt River Exits Durkee Basin
Elevation (m)
Distance (m)
1500
1400
1300
1200
1100
1000
900
800
700
0
2000
4000
6000
8000
10000
12000
14000
16000

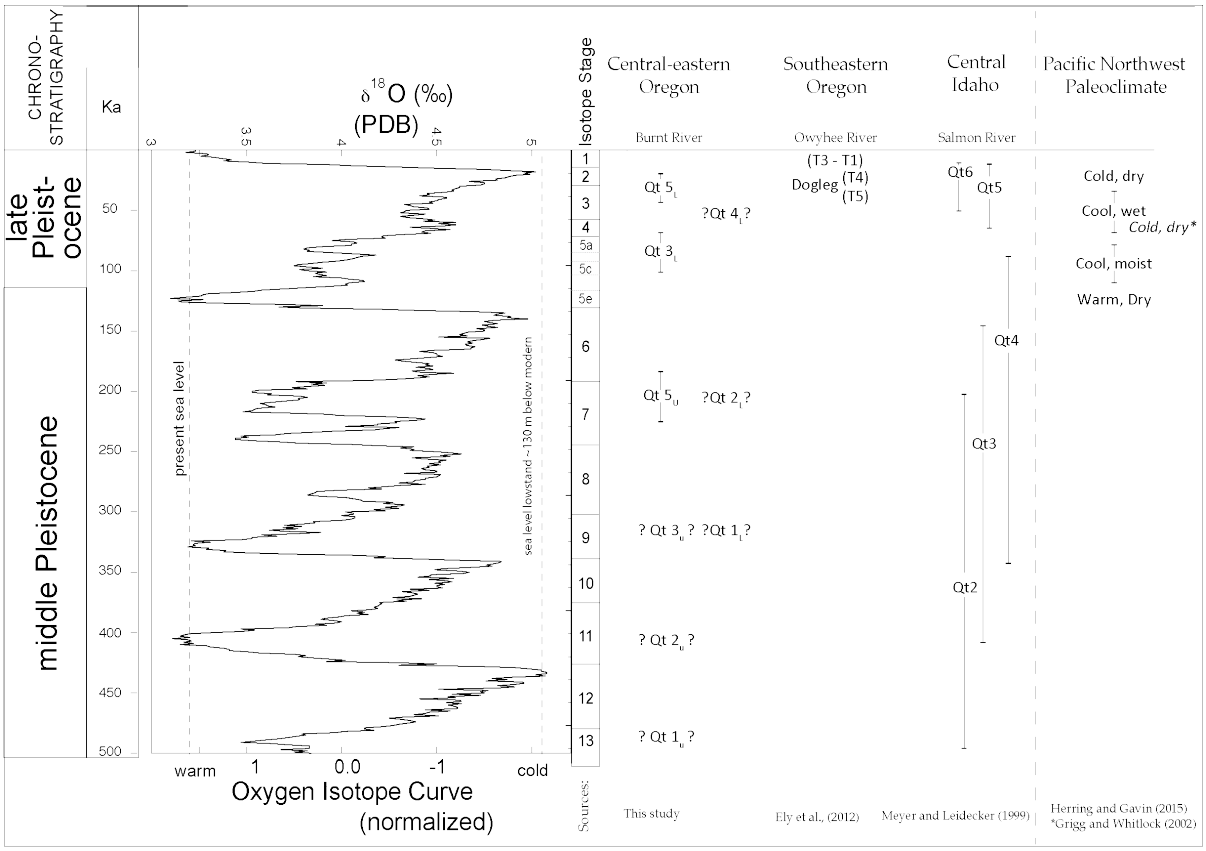

Figure 24. Inferred terrace forming intervals for the Burnt, Owyhee, and the Salmon Rivers. These three rivers provide the only published constraints on terrace formation in eastern Oregon and west-central Idaho. Strath formation appears to take place during warmer, moist interglacial intervals when stream behavior favors enhanced horizontal incision (valley widening and strath cutting) versus vertical incision, which either takes place at the transition from interglacial to glacial or during glacial periods. The Oxygen isotope curve is from Lisiecki and Raymo (2005).

REFERENCES

Allen, J.E., 1991, The Case of the Inverted Auriferous paleotorrents: Oregon Geology, v. 53, p. 104–107.

Ashley, R.P., 1995, Petrology and deformation history of the Burnt River Schist and associated plutonic rocks in the Burnt River canyon area, northeastern Oregon, *in* Vallier, T. and Brooks, H.C. eds., Geology of the Blue Mountains Region of Oregon, Idaho, and Washington: U.S. Geological Survey Professional Paper 1438, p. 457–496.

Bailey, D.G., 1990, Geochemistry and petrogenesis of Miocene volcanic rocks in the Powder River Volcanic Field, northeastern Oregon [Ph.D. thesis]: Pullman, Washington State University, 341 p.

Barry, T.L., Kelley, S.P., Reidel, S.P., Camp, V.E., Self, S., Jarboe, N.A., Duncan, R.A., and Renne, P.R., 2013, Eruption chronology of the Columbia River Basalt Group, *in* Reidel, S.P., Camp, V.E., Ross, M.E., Wolff, J.A., Martin, B.S., Tolan, T.L., and Wells, R.E. eds., The Columbia River Flood Basalt province: Geological Society of America Special Paper 497, p. 45–66.

Becker, T.W., Faccenna, C., Humphreys, E.D., Lowry, A.R., and Miller, M.S., 2013, Static and dynamic support of western United States topography: Earth and Planetary Science Letters, v. 402, p. 234–246.

Braun, J., 2010, The many surface expressions of mantle dynamics: Nature Geoscience, v. 3, p. 825–833.

Brooks, H.C., 1979a, Geologic map of the Huntington and part of the Olds Ferry quadrangles, Baker and Malheur Counties, Oregon: Oregon Department of Geologic and Mineral Industries Geologic Map Series GMS-13, scale 1:62,500.

Brooks, H.C., 1979b, Geologic map of the Oregon part of the Mineral Quadrangle: Oregon Department of Geologic and Mineral Industries Geologic Map Series GMS-12, scale 1:62,500.

Bull, W.B., 1990, Stream-terrace genesis: Implications for soil development: Geomorphology, v. 3, p. 351–367.

Bull, 1991, Geomorphic Responses to Climatic Change: New York, Oxford University Press, 326 p.

Bull, W.B., 2009, Tectonic Geomorphology of Mountains: A New Approach to Paleoseismology: Hoboken, Wiley-Blackwell, 328 p.

Camp, V.E., and Ross, E.M., 2004, Mantle dynamics and genesis of mafic magmatism in the intermontane Pacific Northwest: Journal of Geophysical Research, v. 109, p. BO8204.

Camp, V.E., and Hanan, B.B., 2008, A plume-triggered delamination origin for the Columbia River Basalt Group: Geosphere, v. 4, p. 480.

Cook, K.L., Turowski, J.M., and Hovius, N., 2013, A demonstration of the importance of bedload transport for fluvial bedrock erosion and knickpoint propagation: Earth Surface Processes and Landforms, v. 38, p. 683–695.

Cowan, D.S., and Reiners, P.W., 2004, Age and provenance of lower tertiary fluvial strata, Elkhorn Mountains, E. Oregon: Geological Society of America Abstracts with Programs, Vol. 36, No. 4, p. 34.

Crandell, D.R., 1967, Glaciation at Wallowa Lake, Oregon: U.S. Geological Survey Professional Paper, v. 575, p. 145–153.

Cummings, M.L., Evans, J.G., Ferns, M.L., and Lees, K.R., 2000, Stratigraphic and structural evolution of the middle Miocene synvolcanic Oregon-Idaho graben: Bulletin of the Geological Society of America, v. 112, p. 668–682.

Darold, A., and Humphreys, E., 2013, Upper mantle seismic structure beneath the Pacific Northwest: A plume-triggered delamination origin for the Columbia River flood basalt eruptions: Earth and Planetary Science Letters, v. 365, p. 232–242.

D'Agostino, N., Jackson, J. A., Dramis, F., and Funiciello, R., 2001, Interactions between mantle upwelling, drainage evolution and active normal faulting: An example from the Central Appennines (Italy): Geophysical Journal International, v. 147, p. 475–497.

Dawers, N.H., Anders, M.H., and Scholz, C.H., 1993, Growth of normal faults: Displacement-length scaling: Geology, v. 21, p. 1107–1110.

DeCelles, P.G., 2004, Late Jurassic to Eocene evolution of the Cordillera: American Journal of Science, v. 304, p. 105–168.

Dorsey, R. J., and LaMaskin, T. A., 2007, Basinal response to Triassic-Jurassic collisional tectonics in the Blue Mountains Province, northeastern Oregon: American Journal of Science, v. 307, p. 1167–1193.

Dorsey, R. J., and Lamaskin, T.A., 2008, Mesozoic collision and accretion of oceanic terranes in the Blue Mountains Province of northeastern Oregon: New insights from the stratigraphic record: Arizona Geological Society Digest, v. 22, p. 325–332.

Duncan, R.A., 1982, A capture island chain in the Coast Range of Oregon and Washington: Journal of Geophysical Research, v. 87, p. 10827–10837.

Ely, L.L., Brossy, C.C., House, P.K., Safran, E.B., O'Connor, J.E., Champion, D.E., Fenton, C.R., Bondre, N.R., Orem, C.A., and Grant, G.E., 2012, Owyhee River intracanyon lava flows: Does the river give a dam?: Geological Society of America Bulletin, v. 124, p. 1667-1687.

Ferns, M.L., and McClaughry, J.D., 2013, Stratigraphy and volcanic evolution of the middle Miocene to Pliocene La Grande – Owyhee eruptive axis in eastern Oregon: The Columbia River Flood Basalt province: Geological Society of America Special Paper 497, p. 401–427.

Ferns, .M.L., Mcconnell, V.S., and Madin, I.P., 2010, Geology of the Upper Grande Ronde River Basin, Union County, Oregon: Oregon Department of Geology and Mineral Industries Bulletin 107, scale 1:100,000, 1 sheet, 65 p text.

Finnegan, N.J., and Dietrich, W.E., 2011, Episodic bedrock strath terrace formation due to meander migration and cutoff: Geology, v. 39, p. 143–146.

Gallen, S.F., Pazzaglia, F.J., Wegmann, K.W., Pederson, J., and Gardner, T.W., 2015, The influence of a dynamic reference frame on temporal signals of river incision: Geology, v. 39, p. 623-626.

Gallen, S.F., Wegmann, K.W., and Bohnenstiehl, D.R., 2013, Miocene rejuvenation of topographic relief in the Southern Appalachians: GSA Today, v. 23, p. 4–10.

Gao, H., Humphreys, E.D., Yao, H., and van der Hilst, R.D., 2011, Crust and lithosphere structure of the northwestern U.S. with ambient noise tomography: Terrane accretion and Cascade arc development: Earth and Planetary Science Letters, v. 304, p. 202–211.

Gaschnig, R.M., Vervoort, J.D., Lewis, R.S., and McClelland, W.C., 2010, Migrating magmatism in the northern US Cordillera: In situ U-Pb geochronology of the Idaho batholith: Contributions to Mineralogy and Petrology, v. 159, no. 6, p. 863–883.

Gile, L.H., Peterson, F.F., and Grossman, R.B., 1965, The K Horizon: A master soil horizon of carbonate accumulations: Soil Science, v. 99, p. 74–82.

Grigg, L.D., and Whitlock, C., 2002, Patterns and causes of millenial-scale climate change in the Pacific Northwest during the last glacial period: Quaternary Science Reviews, v. 21, p. 2067–2083.

Hales, T.C., Abt, D.L., Humphreys, E.D., and Roering, J.J., 2005, A lithospheric instability origin for Columbia River flood basalts and Wallowa Mountains uplift in northeast Oregon: Nature, v. 438, p. 842–53.

Hancock, G.S., and Anderson, R.S., 2002, Numerical modeling of fluvial strath-terrace formation in response to oscillating climate: Geological Society of America Bulletin, v. 114, p. 1131-1142.

Herring, E.M., and Gavin, D.G., 2015, Climate and vegetation since the Last Interglacial (MIS 5e) in a putative glacial refugium, northern Idaho, USA: Quaternary Science Reviews, v. 117, p. 82–95.

Hooper, P., 1982, The Columbia River Basalts: Science, v. 215, p. 1463–1468.

Hooper, P., and Swanson, D.A., 1990, Columbia River Basalt Group and associated volcanic rocks of the Blue Mountains province, *in* Walker, G.P., Robinson, P.T., Hooper, P.R., Swanson, D.A., and McKee, E.H., eds., The geology of the Blue Mountains region of Oregon, Idaho, and Washington; Cenozoic geology of the Blue Mountains region, U.S. Geological Survey Professional Paper 1437, p. 63–99.

Hooper, P.R., Binger, G.B., and Lees, K.R., 2002, Ages of the Steen and Columbia River flood basalts and their relationship to extension-related calc-alkalic volcanism in eastern Oregon: Geological Society Of America Bulletin, v. 114, p. 923–924.

Hooper, P.R., Camp, V.E., Reidel, S.P., and Ross, M.E., 2007, The origin of the Columbia River flood basalt province: Plume versus nonplume models, *in* Foulger, G.R., and Jordy, P.M., eds., Plates, plumes, and planetary processes: Geological Society of America Special Paper 430, p. 635–668.

Hopper, E., Ford, H. A., Fischer, K.M., Lekic, V., and Fouch, M.J., 2014, The lithosphere-asthenosphere boundary and the tectonic and magmatic history of the northwestern United States: Earth and Planetary Science Letters, v. 1, p. 1–13.

Humphreys, E.D., 1995, Post-Laramide removal of the Farallon slab, western United States: Geology, v. 23, p. 987–990.

Johnson, D.M., Hooper, P.R., and Conrey, R.M., XRF Analysis of Rocks and Minerals and Trace Elements on a Single Low Dilution Li-tetraborate Fused Bead: Advances in X-ray Analysis, v. 41, p. 843 – 867.

Keller, E.A., and Pinter, N., 2002, Active Tectonics: Earthquakes and Landscape: Upper Saddle River, Prentice Hall, 362 p.

Kirby, E., and Whipple, K., 2001, Quantifying differential rock-uplift rates via stream profile analysis: Geology, v. 29, p. 415–418.

Kirby, E., Whipple, K.X., Tang, W., and Chen, Z., 2003, Distribution of active rock uplift along the eastern margin of the Tibetan Plateau: Inferences from bedrock channel longitudinal profiles: Journal of Geophysical Research, v. 108 B4, p. 2217.

Kuehn, S.C., and Negrini, R.M., 2010, A 250 k.y. record of Cascade arc pyroclastic volcanism from late Pleistocene lacustrine sediments near Summer Lake, Oregon, USA: Geosphere, v. 6, p. 397–429.

Lamaskin, T.A., Schwartz, J.J., Tikoff, B., and Lewis, R.S., 2014, Geology and geophysics of the greater Blue Mountains Province, Salmon River Belt, and Western Idaho Shear Zone: Late Paleozoic through Cenozoic evolution of a key location of the Cordilleran Orogen: Geological Society of America Abstracts with Programs, v. 46, no. 5, p. 14.

Lamaskin, T.A., Vervoort, J.D., Dorsey, R.J., and Wright, J.E., 2009, Early Mesozoic paleogeography and tectonic evolution of the western United States: Insights from detrital zircon U-Pb geochronology, Blue Mountains Province, northeastern Oregon: Geological Society of America Bulletin, v. 123, p. 1939–1965.

Leeman, W.P., Oldow, J.S., and Hart, W.K., 1992, Lithosphere-scale thrusting in the western U.S. Cordillera as constrained by Sr and Nd isotopic transitions in Neogene volcanic rocks: Geology, v. 20, p. 63-66.

Lisiecki, L.E., and Raymo, M.E., 2005, A Pliocene-Pleistocene stack of 57 globally distributed benthic $d^{18}O$ records: Paleogeography, v. 20, p PA1003.

Lyle, M., Heusser, L., Herbert, T., Mix, A., and Barron, J., Interglacial theme and variations: 500 k.y. of orbital forcing and associated responses from the terrestrial and marine biosphere, U.S. Pacific Northwest: Geology, v. 29, n. 12, p. 1115–1118.

Markey, B.G., Bøtter-Jensen, L., and Duller, G.A., 1997, A new flexible system for measuring thermally and optically stimulated luminescence: Radiation Measurements, v. 27, p. 83–90.

McCaffrey, R., King, R.W., Payne, S.J., and Lancaster, M., 2013, Active tectonics of northwestern U.S. inferred from GPS-derived surface velocities: Journal of Geophysical Research: Solid Earth, v. 118, p. 709–723.

McClaughry, J.D., Gordon, C.L., and Ferns, M.L., 2009, Field trip guide to the middle Eocene Wildcat Mountain Caldera , Mountain: Oregon Geology, v. 69, no 1, p. 5–24.

McClaughry, J.D., Ferns, M.L., and Gordon, C.L., 2014, Geologic Evolution of the Middle Eocene Wildcat Mountain Caldera, Central Oregon, USA: Geological Society of America Abstracts with Programs, v. 46, no. 4, p. 72.

McDonald, E. V., Sweeney, M.R., and Busacca, A.J., 2012, Glacial outburst floods and loess sedimentation documented during Oxygen Isotope Stage 4 on the Columbia Plateau, Washington State: Quaternary Science Reviews, v. 45, p. 18–30.

Meyer, G.A., and Leidecker, M.E., 1999, Fluvial terraces along the Middle Fork Salmon River, Idaho, and their relation to glaciation, landslide dams, and incision rates: A preliminary analysis and river-mile guide *in* Hughes S.S., and Thackray, G.D., eds., Guidebook to the Geology of Eastern Idaho, Pocatello, Id, Idaho Museum of Natural History, p. 219-235.

Miller, D.M., Nilsen, T.H., and Bilodeau, W.L., 1992, Late Cretaceous to Early Eocene geologic evolution of the U.S. Cordillera, *in* Burchfiel, B.C., Lipman, P.W., and Zoback, M.L. eds., The Cordilleran Orogen: Conterminous U.S.: Boulder, Colorado, Geological Society of America, Geology of North America, v. G-3, p. 205-260

Miller, S.R., Sak, P.B., Kirby, E., and Bierman, P.R., 2013, Neogene rejuvenation of central Appalachian topography: Evidence for differential rock uplift from stream profiles and erosion rates: Earth and Planetary Science Letters, v. 369-370, p. 1–12.

Mix, H.T., Mulch, A., Kent-Corson, M.L., and Chamberlain, C.P., 2011, Cenozoic migration of topography in the North American Cordillera: Geology, v. 39, p. 87–90.

Montgomery, D.R., 2004, Observations on the role of lithology in strath terrace formation and bedrock channel width: American Journal of Science, v. 304, p. 454–476.

Murray, A.S., and Wintle, A.G., 2000, Luminescence dating of quartz using an improved single-aliquot regenerative-dose protocol: Radiation Measurements, v. 32, p. 57-73.

Nicolaysen, K., Ferguson, L., Cohen, A., Lackey, J.S., Bindeman, I., and Ferns, M., 2014, The significance of contemporaneous olivine basalts and basanites to Columbia River

Basalt group genesis - evidence for lithospheric delamination?: Geological Society of America Abstracts with Programs, Vancouver, B.C., v. 46, no. 6, p. 58.

Pazzaglia, F.J., and Brandon, M.T., 2001, A fluvial record of rock uplift and shortening across the Cascadia forearc high: American Journal of Science, v. 301, p. 385-431.

Pazzaglia, F., 2013, Fluvial terraces, *in* Shroder, J., and Wohl, E., eds., Treatise on Geomorphology, Volume 9, Fluvial Geomorphology: San Diego, CA, Academic Press, p. 379-412.

Pederson, J.L., Anders, M.D., Rittenhour, T.M., Sharp, W.D., Gosse, J.C., and Karlstrom, K.E., 2006, Using fill terraces to understand incision rates and evolution of the Colorado River in eastern Grand Canyon, Arizona: Journal of Geophysical Research: Earth Surface, v. 111, p. 1–10.

Pederson, J.L., Cragun, W.S., Hidy, A.J., Rittenour, T.M., and Gosse, J.C., 2013, Colorado River chronostratigraphy at Lee's Ferry, Arizona, and the Colorado Plateau bull's-eye of incision: Geology, v. 41, p. 427–430.

Pierce, K.L., and Morgan, L. A., 2009, Is the track of the Yellowstone hotspot driven by a deep mantle plume? – Review of volcanism, faulting, and uplift in light of new data: Journal of Volcanology and Geothermal Research, v. 188, p. 1–25.

Pierce, K.L., and Morgan, L. A., 1992, The track of the Yellowstone hot spot: Volcanism, faulting, and uplift, *in* Link, P.K., Kuntz, M.A., and Platt, L.W. eds., Regional geology of eastern Idaho and western Wyoming: Geological Society of America Memoir 179, p. 1–53.

Pike, R.J., and Wilson, S.E., 1971, Elevation-relief ratio, hypsometric integral, and geomorphic area-altitude analysis: Geological Society of America Bulletin, v. 82, p. 1079–1084.

Prescott, J.R., and Hutton, J.T., 1994, Cosmic ray contributions to dose rates for luminescence and ESR dating: Large depths and long-term time variations: Radiation Measurements, v. 23, p. 497–500.

Reidel, S.P., Camp, V.E., Tolan, T.L., and Martin, B.S., 2013, The Columbia River flood basalt province *in* Reidel, S.P., Camp, V.E., Ross, M.E., Wolff, J.A., Martin, B.S., Tolan, T.L., and Wells, R.E. eds., The Columbia River Flood Basalt province: Geological Society of America Special Papers, v. 497, p. 1–43.

Reidel, S.P., and Tolan, T.L., 2013a, The Grande Ronde Basalt, Columbia River Basalt Group *in* Reidel, S.P., Camp, V.E., Ross, M.E., Wolff, J.A., Martin, B.S., Tolan, T.L.,

and Wells, R.E. eds., The Columbia River Flood Basalt province: Geological Society of America Special Papers, v. 497, p. 117 – 153.

Reidel, S.P., and Tolan, T.L., 2013b, The late Cenozoic evolution of the Columbia River system in the Columbia River flood basalt province, *in* Reidel, S.P., Camp, V.E., Ross, M.E., Wolff, J.A., Martin, B.S., Tolan, T.L., and Wells, R.E. eds., The Columbia River Flood Basalt province: Geological Society of America Special Paper 497, p. 201–213.

Robyn, T.L., 1977, Geology and petrology of the Strawberry Volcanics, NE Oregon [Ph.D. Thesis]: Eugene, University of Oregon, 224 p.

Rodriguez, S., and Sen, G., 2013, Eruption of the Grande Ronde Basalt lavas, Columbia River Basalt Group: Results of numerical modeling, *in* Hooper, P.R., Camp, V.E., Reidel, S.P., and Ross, M.E. eds., The Columbia River Flood Basalt province: Geological Society of America Special Paper 497, Geologic Society of America, p. 259–272.

Schmandt, B., and Humphreys, E., 2011, Seismically imaged relict slab from the 55 Ma Siletzia accretion to the northwest United States: Geology, v. 39, p. 175–178.

Schwanghart, W., and Scherler, D., 2014, Short Communication: TopoToolbox 2 – MATLAB-based software for topographic analysis and modeling in Earth surface sciences: Earth Surface Dynamics, v. 2, p. 1–7.

Sears, J.W., 2014, Tracking a big Miocene river across the Continental Divide at Monida Pass, Montana/Idaho, *in* Shaw, C.A. and Tikoff, B. eds., Exploring the Northern Rocky Mountains: Geological Society of America Field Guide 37, p. 89–99.

Silberling, N.J., 1987, Lithotectonic terrane map of the western conterminous United State: Miscellaneous Field Studies Map, Series 1874: C1–C43 p.

Stein, R.S., King, G.C.P., and Rundle, J.B., 1988, The growth of geological structures by repeated earthquakes 2. Field examples of continental dip-slip faults: Journal of Geophysical Research, v. 93, p. 13319–13331.

Streck, M., Ferns, M.L., Ricker, C., and Steiner, A., 2011, The Dinner Creek Tuff and other mid-Miocene rhyolites at the magmatic focal zone of the Columbia River Basalt Group: Geological Society of America Abstracts with Programs, v. 43, no. 4, p. 5.

Srivastava, P., Brook, G.A., and Marais, E., Depositional environment and luminescence chronology of the Hoarusib River Clay Castles sediments, northern Namib Desert, Namibia: Catena, v. 59, p. 221-238

Van Tassell, J., Ferns, M., McConnell, V., and Smith, G., 2001, The mid-Pliocene Imbler fish fossils, Grande Ronde Valley, Union County, Oregon , and the connection between Lake Idaho and the Columbia River: Oregon Geology, v. 63, p. 77–96.

Vallier, T., 1998, Islands and Rapids: Lewiston, Confluence Press, 151 p.

Wegmann, K.W., and Pazzaglia, F.J., 2002, Holocene strath terraces, climate change, and active tectonics: The Clearwater River basin, Olympic Peninsula, Washington State: Geological Society of America Bulletin, v. 114, p. 731–744.

Wegmann, K.W., and Pazzaglia, F.J., 2009, Late Quaternary fluvial terraces of the Romagna and Marche Apennines, Italy: Climatic, lithologic, and tectonic controls on terrace genesis in an active orogen: Quaternary Science Reviews, v. 28, p. 137–165.

Wegmann, K.W., Zurek, B.D., Regalla, C. a., Bilardello, D., Wollenberg, J.L., Kopczynski, S.E., Ziemann, J.M., Haight, S.L., Apgar, J.D., Zhao, C., and Pazzaglia, F.J., 2007, Position of the Snake River watershed divide as an indicator of geodynamic processes in the greater Yellowstone region, western North America: Geosphere, v. 3, p. 272.

Wells, D.L., and Coppersmith, K.J., 1994, New empirical relationships among magnitude, rupture length, rupture width, rupture area, and surface displacement: Bulletin of Seismological Society of America, v. 84, p. 974–1002.

Wheeler, H., and Cook, E., 1954, Structural and stratigraphic significance of the Snake River capture, Idaho-Oregon: The Journal of Geology, v. 62, p. 525–536.

Whitlock, C., and Bartlein, P.J., 1997, Vegetation and climate change in northwest America during the past 125 kyr: Nature, v. 388, p. 57–61.

Williams, S.K., 1994, Late Cenozoic tephrastratigraphy of deep sediment cores from the Bonneville Basin, northwest Utah: Geological Society of America Bulletin, v. 106, p. 1517–1530.

Wobus, C., Whipple, K.X., Kirby, E., Snyder, N., Johnson, J., Spyropolou, K., Crosby, B., and Sheehan, D., 2006, Tectonics from topography: procedures, promise, and pitfalls: Geological Society of America Special Paper 398, p. 55–74.

Wolman, M.G., and Miller, J.P., 1960, Magnitude and frequency of forces in geomorphic processes: The Journal of Geology, v. 68, p. 54–74.

Wood, S.H., and Clemens, D.M., 2002, Geologic and tectonic history of the western Snake River Plain, Idaho and Oregon: Idaho Geological Survey Bulletin, v. 30, p. 69-103.

Xue, M., and Allen, R., 2006, Origin of the Newberry Hotspot Track: Evidence from shear-wave splitting: Earth and Planetary Science Letters, v. 244, p. 315–322.

Zaprowski, B.J., Evenson, E.B., Pazzaglia, F.J., and Epstein, J.B., 2001, Knickzone propagation in the Black Hills and northern High Plains: A different perspective on the late Cenozoic exhumation of the Laramide Rocky Mountains: Geology, v. 29, p. 547–550.

APPENDIX

Appendix A. Location and elevation above the modern river for each bedrock strath surface identified during mapping as determined by differential GPS and laser range finder.

Terrace ID	Latitude (° N)	Longitude (° W)	Elevation (m a.s.l.)	Vertical Precision (cm)	Height Above M.R. (m)
BR1	44.35749545	117.2485151	644.116	10	
BR12R	44.35930224	117.2767343	665.534	180	
BR13R	44.38332512	117.3064739	677.051	30	
BR14R1	44.40200253	117.3074083	687.246	30	
BR14R2	44.39936671	117.3074237	675.717	30	7
BR14R3	44.40448875	117.3100971	688.376	110	
BR15R1	44.44385884	117.3270185	707.849	40	
BR15R2	44.44527062	117.3277257	700.629	30	
BR16R	44.39689875	117.3085697	713.741	30	44
BR17R1	44.4496461	117.3304925	710.914	10	
BR18R	44.44615947	117.3262996	698.351	60	
BR19R2	44.46266853	117.3353294	714.483	10	
BR20R	44.47450817	117.3375414	735.267	40	
BR21R	44.4722197	117.3350448	714.231	10	14
BR21R3	44.47319691	117.3344572	760.657	130	56
BR22R2	44.4817502	117.337885	855.303	30	
BR23R2	44.48858988	117.3466668	734.45	90	
BR23R3	44.48637327	117.3464633	762.726	160	
BR24R1	44.48611336	117.348987	728.049	10	
BR24R2	44.49266416	117.3564327	833.442	160	
BR25R1	44.48697946	117.361031	740.465	10	12
BR26R1	44.49918487	117.3684794	767.633	30	32
BR26R2	44.50152042	117.3663139	769.447	180	
BR28R1	44.49938717	117.3716098	738.244	50	3.4
BR29B	44.51167355	117.3733327	822.801	110	83.7
BR31R	44.52266441	117.396065	795.886	10	42
BR32R1	44.53511335	117.4135658	818.229	10	47
BR33R1	44.57286359	117.5206966	841.89	80	
BR34R1	44.5758529	117.5372068	854.367	10	6
BR44R3	44.57703299	117.5424883	866.271	250	
BR37R1	44.56824473	117.6016645	954.721	10	
BR38R1	44.569877	117.591458	952.785	130	22
BR39R1	44.56142273	117.6120617	963.421	30	26
BR40R	44.56093881	117.6118546	939.008	160	
BR41R1	44.55334375	117.6242128	1002.338	10	54
BR42R1	44.54790008	117.6266698	989.285	20	40
BR43R3	44.54898719	117.663851	1034.808	180	66.4
BR44R1	44.54549936	117.6808251	981.833	20	8.2
BR44R2	44.54569592	117.68166	997.799	10	25.5
BR45R1	44.53749696	117.6918886	997.443	160	11.5
BR45R2	44.5415784	117.6852744	1038.996	180	54.8
BR45R3	44.54075037	117.687838	1010.335	140	27.6
BR46R1	44.52880383	117.7014588	1003.329	20	12
BR46R2	44.52922634	117.7037347	1043.538	260	50.8
BR46R3	44.52922914	117.7037321	1042.503	220	
BR47R1	44.52431361	117.7108211	1010.208	30	11.4
BR48R1	44.51664824	117.7122672	1030.517	10	20
BR48R2	44.51694461	117.7122832	1023.121	30	
BR50R1	44.51230506	117.71286	1019.451	70	3.1
BR51R1	44.51096519	117.7171937	1034.827	10	13
BR52-4	44.50808941	117.7195396	1032.636	110	12.5
BR52-3	44.51045537	117.7226855	1094.109	120	
BR-52-2	44.50227122	117.7169398	1142.554	150	
BR53-1	44.48336516	117.7492634	1045.089	90	
BR60R	44.54530583	117.6793475	985.446	10	

Appendix B. Geologic Map of the upper Burnt River canyon.

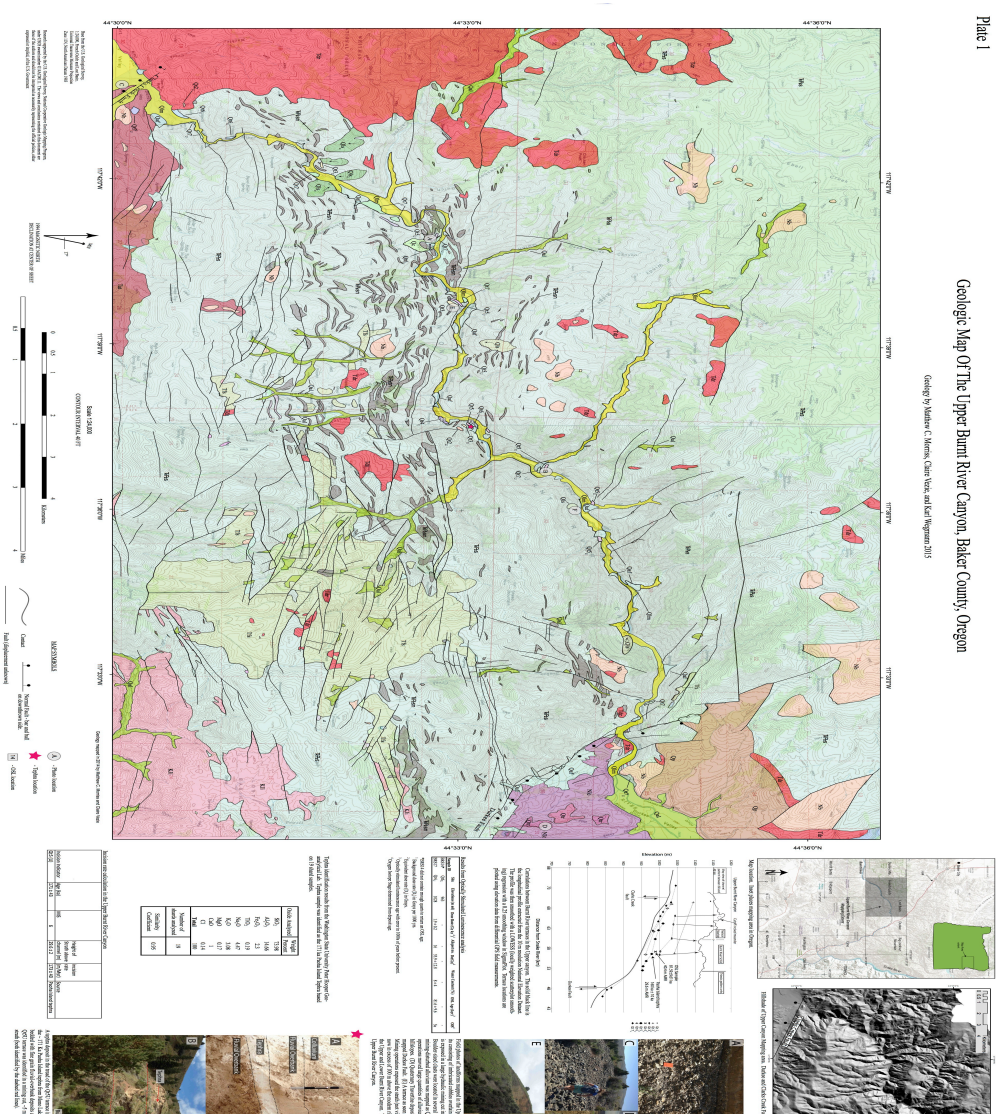

Appendix C. Geologic Map of the Durkee Basin

Appendix D. Geologic Map of lower Burnt River canyon.

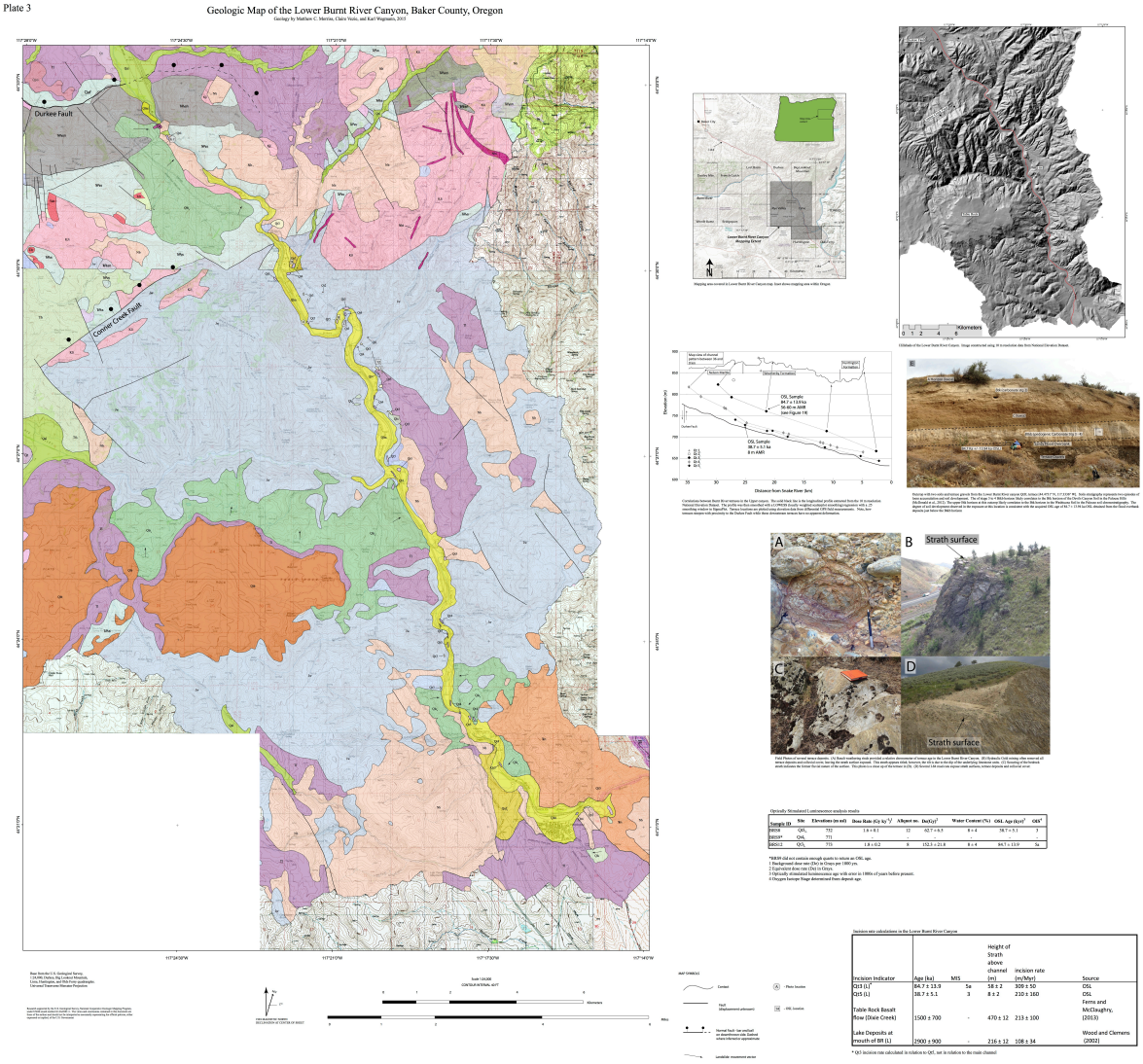

Appendix E. Key for geologic map.